journal of the international meteor organization

WGN

46:4
august 2018

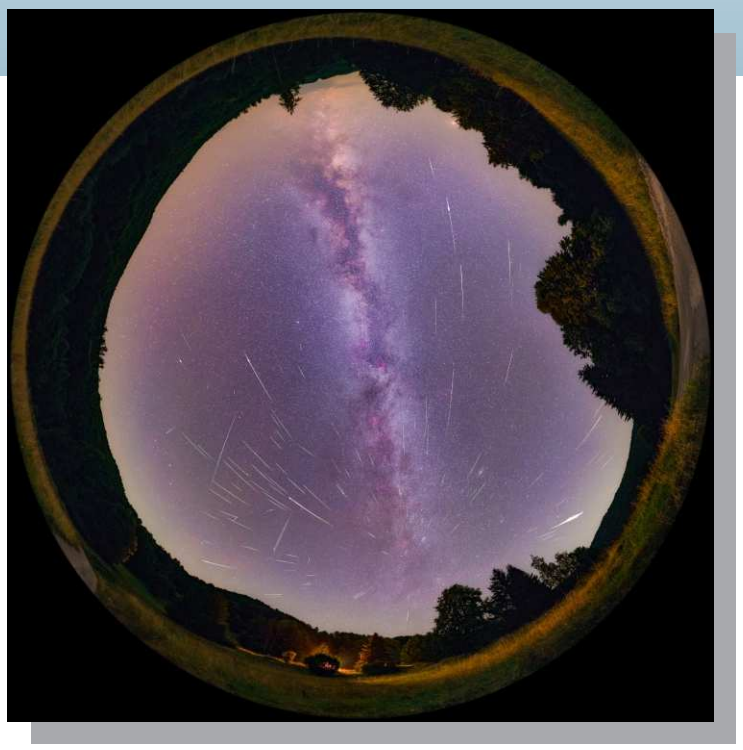

In Memoriam: Dr. Eduard Pittich
First science results from Raspberry Pi-based meteor stations
Consequences of different shower definitions
October–November IMO video meteors

ISSN 1016-3115

WGN Vol. 46, No. 4, August 2018, pp. 111 – 146

Administrative

Meteor science

Preliminary results

Front cover photo

All-sky composite image showing 173 meteors captured from Tepličné, Slovakia, on 2018 August 12/13 and 13/14 by Stanislav Kaniansky, Marek Harman, Ján Mäsiar, and Juraj Škvarka, using 11 different combinations of Canon cameras equipped with lenses ranging from 14 mm to 85 mm. Courtesy of Stanislav Kaniansky and Marek Harman.

Back over photo

Landscape image created from the same individual images as for the front cover image. Courtesy of Stanislav Kaniansky and Marek Harman.

Writing for WGN

This Journal welcomes papers submitted for publication. All papers are reviewed for scientific content, and edited for English and style. Instructions for authors can be found in WGN **45:1**, 1–5, and at `http://www.imo.net/docs/writingforwgn.pdf` .

Copyright

Legal address

International Meteor Organization, Jozef Mattheessensstraat 60, 2540 Hove, Belgium.

In Memoriam: Dr. Eduard Pittich

Juraj Tóth[1]

Received 2018 July 16

Eduard Pittich, a Slovak astronomer working on research of comets and dust particle dynamics, passed away after a few months battle with illness on June 29, 2018 in Bratislava at the age of 78. He was a regular attendee of the IMC.

Eduard Pittich was born in Bratislava in 1940. He graduated in astronomy and astrophysics from Comenius University, Slovakia in 1962 and worked at the Astronomical Institute of the Slovak Academy of Sciences in Bratislava, in the interplanetary matter group, notably with Dr. Ľubomír Kresák, Dr. Ján Štohl, professor Anton Hajduk and professor Vladimír Porubčan until his retirement. He published a catalog of short-period comets (1986) and many other research papers. He was one of the initiators of the construction of the Astronomical and Geophysical Observatory in Modra. He was a member of the IAU. Asteroid (5768) Pittich was named in his honor.

He is survived by his second wife Dr. Nina Solovaya and daughter Dr. Jana Pittichova Chesley, both astronomers. Our thoughts go to them.

[1]Astronomical and Geophysical Observatory Modra, Faculty of Mathematics, Physics and Informatics, Comenius University in Bratislava, Slovakia. Email: Juraj.Toth@fmph.uniba.sk

Figure 1 – Photograph of E. Pittich (on the left), L. Kresák (on the right) and D. Kalmančok (in the middle) in the Astronomical Institute of Slovak Academy of Sciences in Bratislava, March 10, 1978. Author: Štefan Petráš.

Figure 2 – Photograph of E. Pittich on July 26, 2014. Courtesy of: Dr. Jana Pittichova Chesley.

IMO bibcode WGN-464-toth-pittich NASA-ADS bibcode 2018JIMO...46..111T

Meteor science

Compressive strength of a skirting Daytime Arietid – first science results from low-cost Raspberry Pi-based meteor stations

Denis Vida[1,2,3], *Michael J. Mazur*[1,2], *Damir Šegon*[4], *Patrik Kukić*[5], *and Aleksandar Merlak*[6]

We present the first detailed reduction of a double-station meteor recorded solely by a low-cost Raspberry Pi-based meteor system and demonstrate the quality of the data. The reduced event was a Daytime Arietid with an entry angle of only $\sim 1^\circ$ and it lasted for 2.5 s. It had a sun-skirting orbit and it reached an equilibrium temperature of over 1000 K at perihelion. Due to the low entry angle the dynamic pressure on the meteor slowly increased and the compressive strength could be precisely measured. The meteoroid fragmented into a long trail at around 1.3 kPa, a very low compressive strength which indicates a highly porous meteoroid which had its volatiles completely removed due to a high level of thermal processing.

Received 2018 July 3

1 Introduction

Since 2015 there is an ongoing effort to develop a low-cost meteor system based on Raspberry Pi single-board computers which would replace the costly meteor observation systems used today (Zubović et al., 2015). Vida et al. (2016) demonstrated novel meteor and fireball detection algorithms which can run on such computers. Vida et al. (2018b) showed the first observational results, and the quality of astrometric and photometric calibrations, as well as the feasibility of using low-cost CMOS IP cameras for meteor observations. CMOS rolling shutter cameras with the Sony IMX225 sensors (1280×720 resolution, 25 FPS) have yielded a limiting magnitude for stars of +5.5 with a 4 mm $f/1.2$ lens ($64^\circ \times 35^\circ$ FOV) under both dark and light-polluted skies.

A permanent testbed Raspberry Pi Meteor Station (RMS) was installed in June 2017 near Elginfield, Ontario, Canada. In mid-June 2018 a second station was installed near Tavistock (both sites operated by the UWO Meteor Physics Group), the distance between stations is about 45 km. After initial testing, the first orbits using the systems were calculated.

The initial astrometric calibration is performed manually on several tens of stars on a single image, and then automatically refined every night using 1000s of stars recorded throughout the night, up to the precision of 1/3 px (following the procedure of Šegon (2009)). The photometric calibration is done manually – we found that the IMX225 sensors have $\gamma = 1.0$, thus a linear fit between the logarithm of the sum of the star intensity and the star magnitude can be performed, were the line has a slope of -2.5 (by definition), while only the photometric offset is fitted (i.e. the intercept of the line). The calibration procedure is described in detail in Vida et al. (2018b). The photometric offsets were 10.2 and 10.6 for Elginfield and Tavistock, respectfully.

Figure 1 – RMS camera at Tavistock

In this paper we present a detailed reduction of one dynamically and physically interesting event, demonstrate the quality of the data obtained, and present the science potential of the systems.

2 A skirting Daytime Arietid meteor

On 2018 June 15 at $07^h15^m44^s$ UTC (03^h15^m local time), the second night of double-station operation, both stations observed a 2.5 s long meteor which spanned a large portion of fields of view of both cameras. Figures 2 and 3 show co-added images of the meteor from both stations.

After estimating the trajectory on automated astrometry picks using the Borovička (1990) lines of sight method we noticed several peculiarities:

- the entry angle was very low, 0.5°
- the entry angle after the correction for Earth's gravity was around/below 0°
- there was virtually no deceleration
- the meteor climbed back up several tens of meters after the first half of the trajectory

[1]Department of Earth Sciences, University of Western Ontario, London, Ontario, N6A 5B7, Canada.
[2]Department of Physics and Astronomy, University of Western Ontario, London, Ontario, N6A 3K7, Canada.
[3]Email: dvida@uwo.ca
[4]Astronomical Society Istra Pula, Park Monte Zaro 2, HR-52100 Pula, Croatia
[5]XV Gymnasium, Jordanovac 8, HR-10000 Zagreb, Croatia
[6]Istrastream d.o.o., Hum, Croatia

IMO bibcode WGN-464-vida-arietid
NASA-ADS bibcode 2018JIMO...46..113V

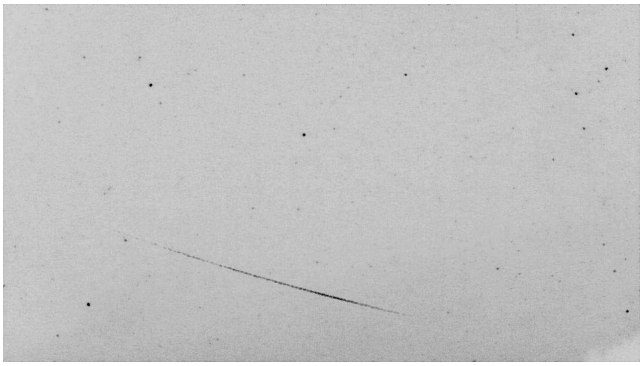

Figure 2 – The image of the event from Elginfield (CA0001). The meteor was moving from right to left. The Polaris is in the upper centre, Cassiopeia is in the upper right.

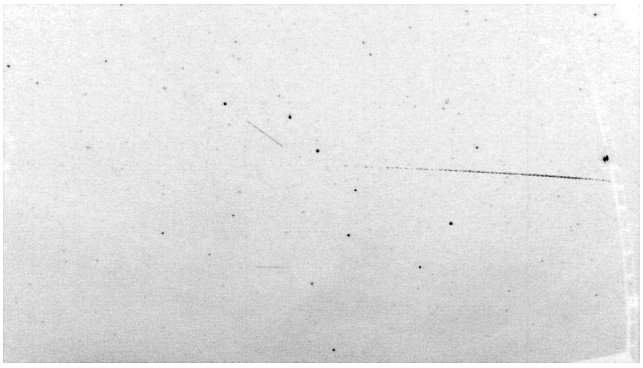

Figure 3 – The image of the event from Tavistock (CA0003). The meteor was moving from right to left. The big dipper dominates the centre of the image. An antenna mast is obstructing view of the beginning of the meteor, and thin clouds were present.

These were all indications of an Earth grazer, thus we decided to perform a more detailed manual reduction of the event using open source tools developed as a part of the RMS software package[a]. Figure 4 shows the manual reduction procedure.

Although Four-frame Temporal Pixel compression was used (Jenniskens et al., 2011), the RMS fireball detector detected the meteor in real time and stored its raw video frames which were showing that the meteor developed a long trail which influenced the positions of automated centroids. Figure 5 shows the mosaics of raw frame cut-outs from the Elginfield station. Due to the horizontal orientation of the meteor on the image and its slow on-chip angular velocity, the centroid correction for the rolling shutter effect was not needed. The effect of a rolling shutter on meteor centroids and the proposed correction will be elaborated in a future paper.

After a careful manual reduction where only the head of the meteor was centroided and the trail was excluded, the entry angle changed to $1.4° \pm 0.2°$, but the gravity-corrected entry angle was still $-0.4° \pm 0.2°$, making it a possible Earth grazer. Nevertheless, after the manual reduction the meteor did not climb up, but always descended down the atmosphere. Despite the ground track of almost 120 km (Figure 6) and the duration of 2.5 s, the meteor ended at 95.8 km, only 2 km below its beginning height. We believe that if the meteoroid was larger, it would have returned to interplanetary space, but it seems that the whole mass ablated away.

[a]Software is available on our GitHub page at: `https://github.com/CroatianMeteorNetwork/RMS`

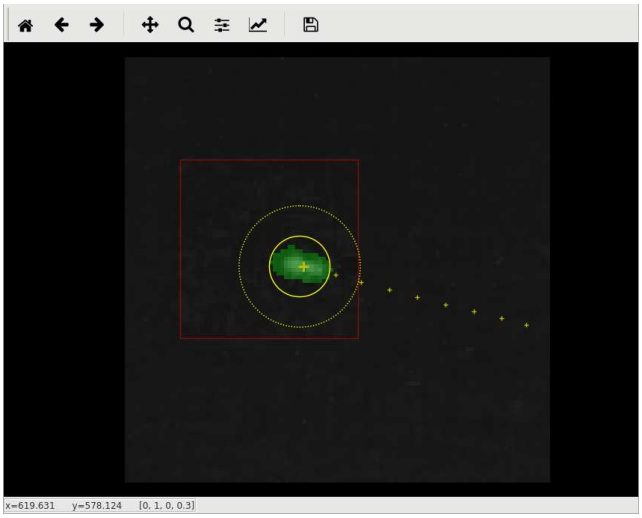

Figure 4 – Manual reduction procedure. The image is zoomed in around the meteor. The yellow circle is the centroiding annulus, the large yellow cross is the centroid on the current frame and small crosses are centroid on previous frames. The green transparent pixels are the pixels included in the photometry, and the red square is the raw frame cut-out.

The indicators of the quality of the reduction are the angular residuals of the trajectory fit shown in Figure 7. The standard deviation of the residuals from both stations is around 1 arc minute, which corresponds to the average precision of the astrometric fit (1/3 px). The scale of the image with the used cameras and lenses is around 3 arc minutes per pixel. The standard deviation of the spatial residuals from both sites was around 40 meters.

The initial velocity was estimated by performing a linear regression on time vs. length of the first 25% of the trajectory. The illustrate the deceleration of the meteor, we compute the lag, i.e. the difference in along-track position between the observed meteor and a hypothetical non-decelerating meteor. Figure 8 shows the observed lag from both stations. The meteor started to decelerate about 0.5 s after detection and stopped decelerating about 1 s after that. Note that the lag from Tavistock (CA0003) does not match the Elginfield lag well in the beginning as the meteor was passing behind a mast which made the determination of its position uncertain. Figure 9 shows the instantaneous velocities of the meteor – note that the velocity does not change much, it is nearly constant at $v = 42\ \mathrm{km\,s^{-1}}$.

The photometry was also performed manually. Every pixel that was a part of the meteor was "colored in" and the sum of the intensity of all marked pixels were taken. The comparison of absolute magnitudes (visual magnitudes normalized to 100 km) is shown in Figure 11. The error bars represent the photometric uncertainty. The two light curves deviate more around the peak brightness of the meteor due to a thin layer of clouds present at Tavistock (CA0003), which led to the underestimation of the brightness of the meteor. The

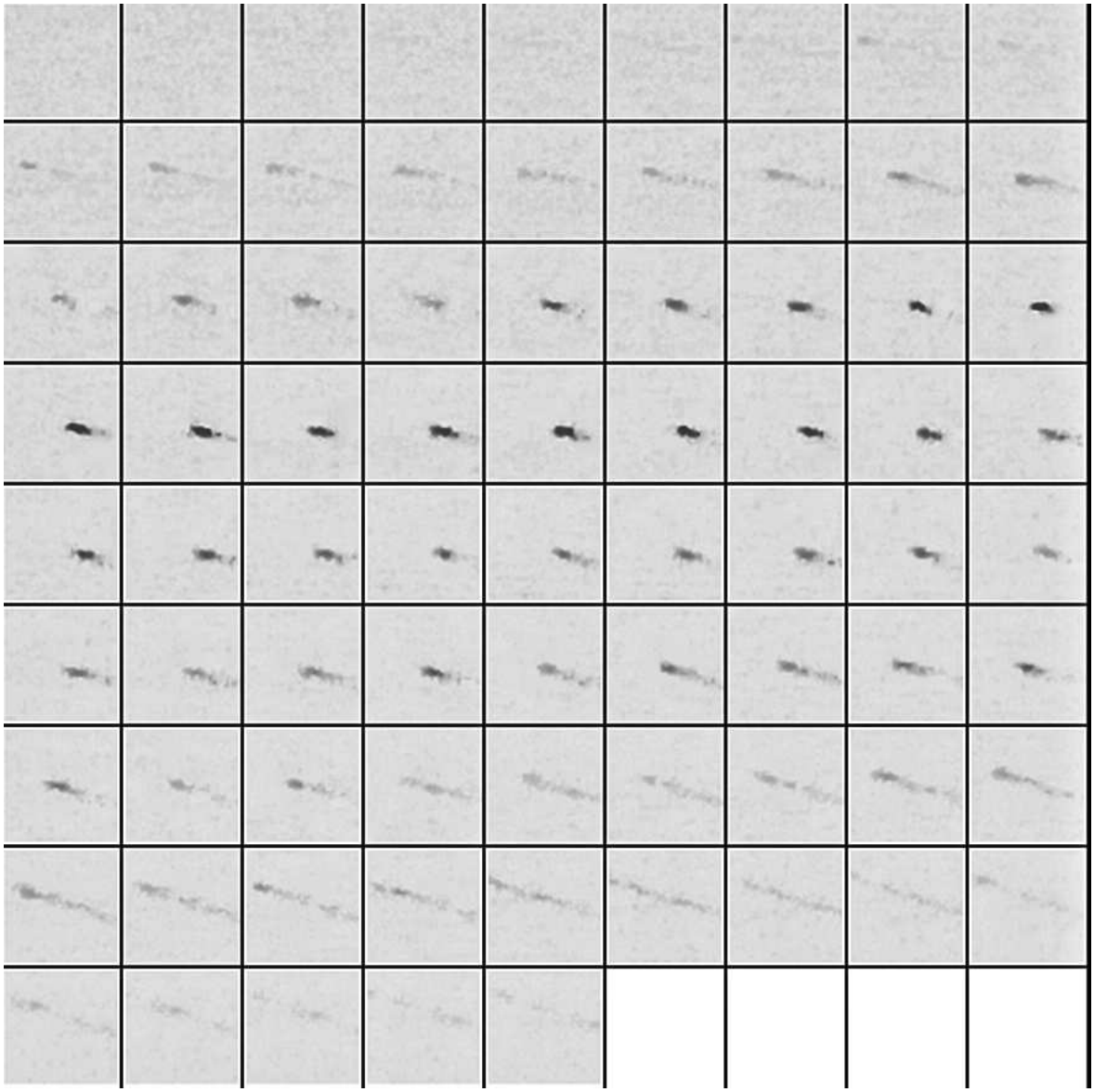

Figure 5 – Raw frame cut-outs from Elginfield. The event is showing a large trail.

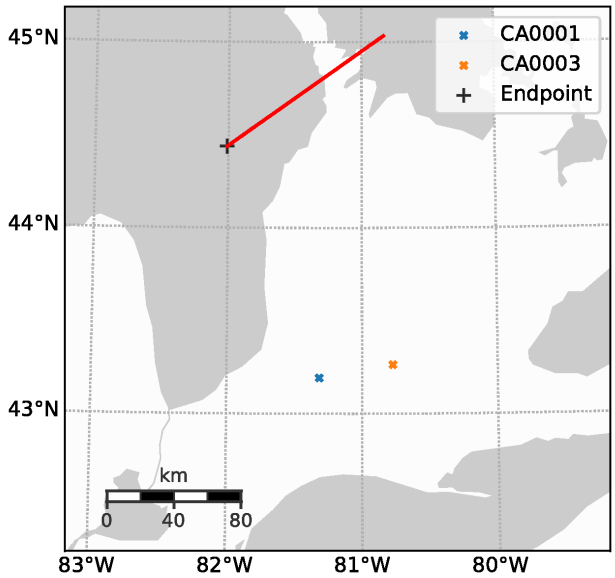

Figure 6 – Ground track of the event. CA0001 is the Elginfield station, and CA0003 is the Tavistock station. Lake Huron is in the upper left, Lake Earie at the bottom.

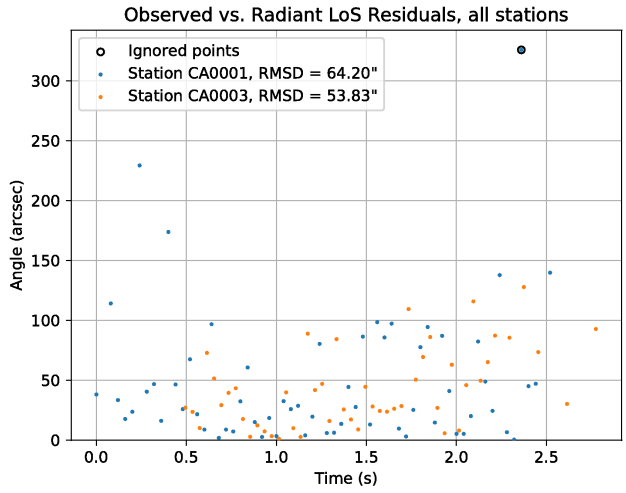

Figure 7 – Angular residuals of the trajectory fit. RMSD is root-mean-square deviation. Note that the deviation is higher at the beginning and the end as the meteor was fainter, thus the centroids were more uncertain due to a lower SNR.

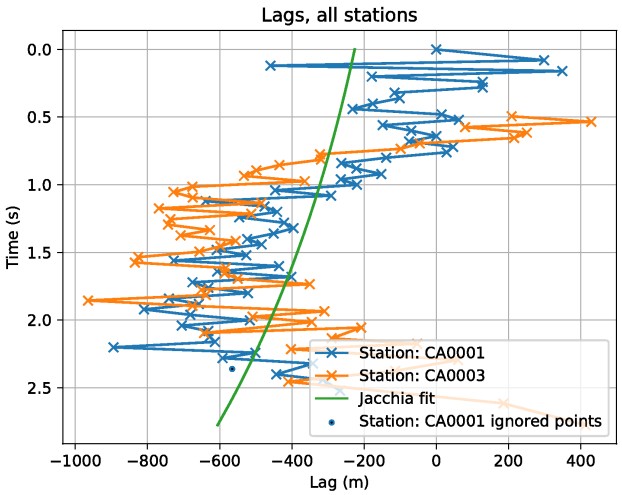

Figure 8 – The lag, i.e. the deceleration profile of the event. An operational fit of the Whipple & Jacchia (1957) exponential deceleration function was performed on the lag, but it does not represent the deceleration well.

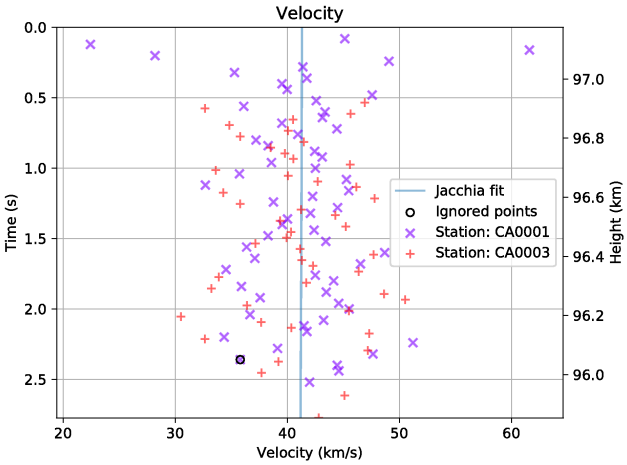

Figure 9 – Instantaneous velocities of the event.

photometric mass of the meteoroid was 0.2 g, assuming a dimensionless luminous efficiency of $\tau = 0.7\%$ and the power of a zero-magnitude meteor of $P_{0M} = 1210$ W (the value is taken for Sony HAD cameras from Weryk & Brown (2013)).

3 The orbit and physical properties of the meteoroid

The orbit of the meteoroid is interesting as well. It is shown in Figure 10 and details are given in Table 1. The uncertainties were estimated by adding Gaussian noise with the standard deviation estimated from the fit residuals (see Figure 7) and refitting the trajectory 100 times. The convergence angle was only 3°, but we are confident in the quality of the trajectory due to the well matching deceleration between both stations. The high uncertainty in declination is due to the limited geometry.

The meteor was a Daytime Arietid coming from the helion source – the shower association was determined

Table 1 – Orbital parameters of the meteoroid

Parameter	Value	Uncertainty
RA_g	48 °.83	±0 °.09
Dec_g	+24 °.01	±0 °.32
V_g	40.57 km s^{-1}	±0.26 km s^{-1}
$\lambda_\odot$	83 °.91	
a	1.96 AU	±0.07 AU
q	0.053 AU	±0.001 AU
e	0.973	±0.001
peri	22 °.58	±0 °.39
node	83 °.92	
i	25 °.53	±1 °.25

using the values from the IAU MDC database[b]. The perihelion distance was only $q = 0.052$ AU, and the eccentricity $e = 0.9734$, which classifies the orbit as a sun-skirter (Jones et al., 2018). The most recent perihelion was on May 13, only 33 days before it was observed. Even assuming a high Bond albedo of the particle of 0.5, the equilibrium temperature of the meteoroid at perihelion reaches over 1000 K, and due to its small size we can assume that is was heated throughout. At these temperatures for millimetre-sized meteoroids, all ices and volatiles sublimate within minutes (Crifo, 1995), leaving only refractory material behind. Furthermore, at the given perihelion of $\sim 11 R_\odot$ (solar radii) it is expected that all iron, magnetite and olivine sublimate too (Mann et al., 2004).

The meteoroid probably originated from comet 96P/Machholz (Abedin et al., 2017). Its significantly smaller semi-major axis indicates significant Poynting-Robertson (PR) evolution. As the period of the meteoroid is only 2.7 years, it had probably undergone multiple perihelion passages and is heavily thermally processed. Furthermore, we note that the estimated semi-major axis of 2 AU is more consistent with Daytime Arietid radar orbits (Brown et al., 2008) than with optical orbits (2.87 AU) (Jenniskens et al., 2018), a peculiarity which Abedin et al. (2017) too attribute to the PR drag that is acting on smaller meteoroids. On the other hand, the high eccentricity is unusual for PR evolved particles, as a more circular orbit would be expected. Nevertheless, PR drag is not as efficient on meteoroids with high eccentricities (Wyatt & Whipple, 1950).

3.0.1 Compressive strength

We use the dynamic pressure exerted on the meteor by the atmosphere at the moment of fragmentation as a proxy for the compressive strength of the meteoroid (Trigo-Rodriguez & Llorca, 2006; Borovička et al., 2007). Due to the low entry angle, the velocity and the height of the meteoroid do not change rapidly, thus the dynamic pressure on the meteoroid can be precisely estimated (Vida et al., 2018a). The dynamic pressure is simply computed as:

[b]IAU MDC database – Daytime Arietids: `http://pallas.astro.amu.edu.pl/~jopek/MDC2007/Roje/pojedynczy_obiekt.php?kodstrumienia=00171`

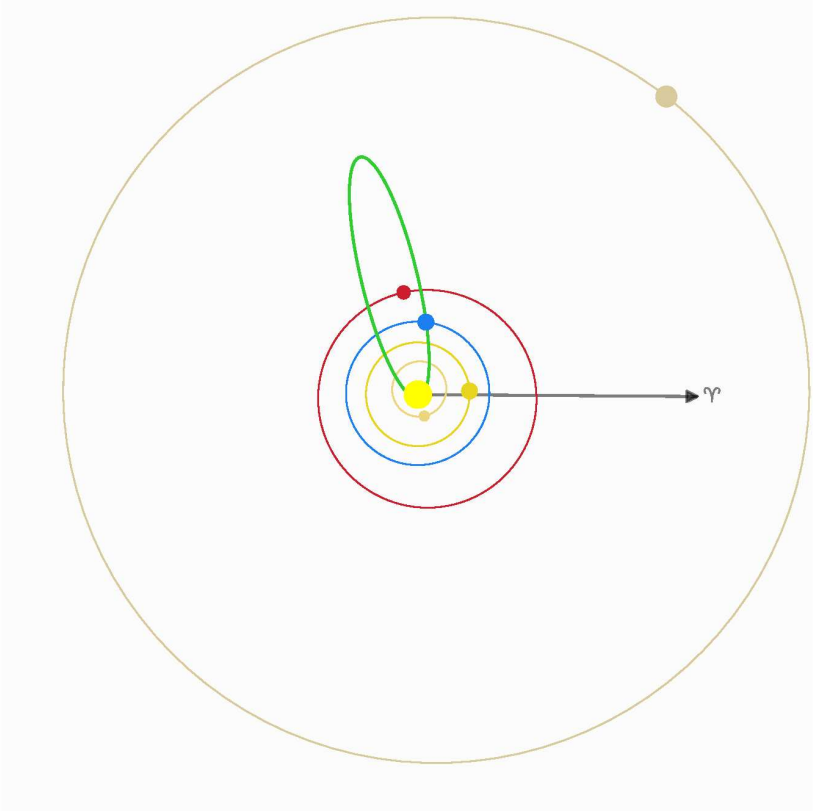

Figure 10 – The orbit of the event is shown in green. The sizes of orbits and planets are not to scale.

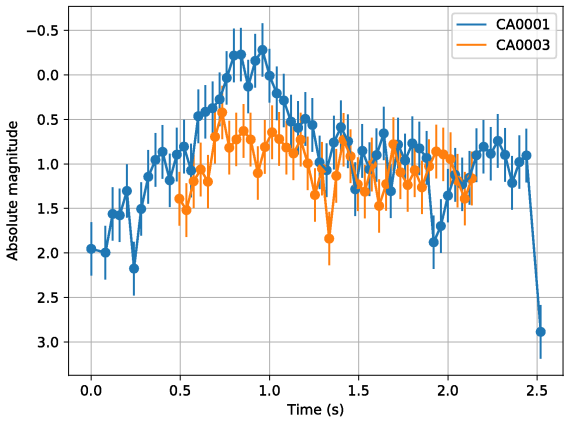

Figure 11 – Light curve of the event.

$$P_{dyn} = \Gamma v^2 \rho_{atm} \quad (1)$$

where Γ is the drag coefficient (assumed to be unity, as in Borovička et al. (2007)), v is the velocity of the meteor at the given point in time, and ρ_{atm} is the atmosphere mass density at the corresponding height. The atmosphere densities were taken from the NRLMSISE-00 atmosphere model (Picone et al., 2002).

At the brightest point on the trajectory, after which the meteor developed a long trail, the dynamic pressure was around 1.3 kPa. We believe that this value reflects the true compressive strength of the meteoroid due to the absence of a volatile matrix which would evaporate at temperatures > 1000 K (Campbell-Brown & Koschny, 2004). Due to such a low strength, the temperature of the meteoroid probably did not exceed the temperature needed to melt silicates, thus the removal of volatiles resulted in a very porous meteoroid which disintegrated after the dynamic pressure exceeded its compressive strength. The long trail might have been caused by thermal erosion (Borovička et al., 2007), but Vida et al. (2018) observed a similar low entry angle event with the Canadian Automated Meteor Observatory's high-resolution mirror tracking system and concluded that the observed distinct fragments separated due to the meteoroid being crushed.

4 Conclusion

We present the first detailed reduction of a double-station meteor using low-cost Raspberry Pi-based meteor stations. The astrometric precision of the cameras is approximately 1 arc minute and the photometric precision is close to 0.2 mag. The reduced meteor was a Daytime Arietid with a very low perihelion distance which had undergone extensive thermal processing at temperatures over 1000 K. As the meteor had a very low entry angle of $\sim 1°$, we were able to precisely measure the compressive strength of the meteoroid. The strength was only 1.3 kPa, an indication of a very weak object comparable to cinder. We believe the meteoroid was a highly porous object (all volatiles absent), and that it experienced a slow mechanical breakup in the atmosphere.

5 Acknowledgements

We thank Peter Gural for reviewing the manuscript of this paper.

6 Author Contributions

DV did the analysis and wrote the paper, MJM helped to install the hardware and reviewed the manuscript, DŠ provided comments and guidance, PK worked on investigating the influence of a rolling shutter on meteor centroids, and AM tested IP cameras and RMS software.

References

Abedin A., Wiegert P., Pokornỳ P., and Brown P. (2017). "The age and the probable parent body of the daytime arietid meteor shower". *Icarus*, **281**, 417–443.

Borovička J., Spurny P., and Koten P. (2007). "Atmospheric deceleration and light curves of Draconid meteors and implications for the structure of cometary dust". *Astronomy & Astrophysics*, **473:2**, 661–672.

Borovička J. (1990). "The comparison of two methods of determining meteor trajectories from photographs". *Bulletin of the Astronomical Institutes of Czechoslovakia*, **41**, 391–396.

Brown P., Weryk R., Wong D., and Jones J. (2008). "A meteoroid stream survey using the Canadian Meteor Orbit Radar: I. Methodology and radiant catalogue". *Icarus*, **195:1**, 317–339.

Campbell-Brown M. and Koschny D. (2004). "Model of the ablation of faint meteors". *Astronomy & Astrophysics*, **418:2**, 751–758.

Crifo J. (1995). "A general physicochemical model of the inner coma of active comets. 1: Implications of spatially distributed gas and dust production". *The Astrophysical Journal*, **445**, 470–488.

Jenniskens P., Baggaley J., Crumpton I., Aldous P., Pokorny P., Janches D., Gural P. S., Samuels D., Albers J., Howell A., et al. (2018). "A survey of southern hemisphere meteor showers". *Planetary and Space Science*.

Jenniskens P., Gural P., Dynneson L., Grigsby B., Newman K., Borden M., Koop M., and Holman D. (2011). "CAMS: Cameras for Allsky Meteor Surveillance to establish minor meteor showers". *Icarus*, **216:1**, 40–61.

Jones G. H., Knight M. M., Battams K., Boice D. C., Brown J., Giordano S., Raymond J., Snodgrass C., Steckloff J. K., Weissman P., et al. (2018). "The science of sungrazers, sunskirters, and other near-sun comets". *Space Science Reviews*, **214:1**, 20.

Mann I., Kimura H., Biesecker D. A., Tsurutani B. T., Grün E., McKibben R. B., Liou J.-C., MacQueen R. M., Mukai T., Guhathakurta M., et al. (2004). "Dust near the Sun". *Space Science Reviews*, **110:3-4**, 269–305.

Picone J., Hedin A., Drob D. P., and Aikin A. (2002). "NRLMSISE-00 empirical model of the atmosphere: Statistical comparisons and scientific issues". *Journal of Geophysical Research: Space Physics*, **107:A12**, SIA–15.

Trigo-Rodriguez J. M. and Llorca J. (2006). "The strength of cometary meteoroids: Clues to the structure and evolution of comets". *Monthly Notices of the Royal Astronomical Society*, **372:2**, 655–660.

Vida D., Brown P., Campbell-Brown M., and Huggins S. (2018a). "Canadian Automated Meteor Observatory: Cometary meteoroid strengths derived from a highly fragmenting event observed on July 21, 2017". In *Proceedings of the International Meteor Conference (IMC2017), Petnica, Serbia*.

Vida D., Mazur M., Šegon D., Zubovič D., Kukič P., Parag F., and Macan A. (2018b). "First results of a Raspberry Pi based meteor camera system". *WGN, Journal of the International Meteor Organization*, **46:2**, 71–78.

Vida D., Zubović D., Šegon D., Gural P., and Cupec R. (2016). "Open-source meteor detection software for low-cost single-board computers". In *Proceedings of the International Meteor Conference (IMC2016), Egmond, The Netherlands*. pages 2–5.

Šegon D. (2009). "How many stars are needed for a good camera calibration?". *WGN, Journal of the International Meteor Organization*, **37:3**, 80–83.

Weryk R. J. and Brown P. G. (2013). "Simultaneous radar and video meteors – II: Photometry and ionisation". *Planetary and Space Science*, **81**, 32–47.

Whipple F. L. and Jacchia L. G. (1957). "The orbits of 308 meteors photographed with super-Schmidt cameras". *The Astronomical Journal*, **62**, 37.

Wyatt S. P. and Whipple F. L. (1950). "The Poynting-Robertson effect on meteor orbits". *The Astrophysical Journal*, **111**, 134–141.

Zubović D., Vida D., Gural P., and Šegon D. (2015). "Advances in the development of a low-cost video meteor station". In *Proceedings of the International Meteor Conference, Mistelbach, Austria*. pages 27–30.

Handling Editor: Javor Kac

This paper has been typeset from a LaTeX file prepared by the authors.

Different definitions make a meteor shower distorted. The views from SonotaCo net and CAMS.

Masahiro Koseki [1]

We compared the raw data of two sets of video observations (SonotaCo Network and CAMS) through 11 meteor showers: Quadrantids, April Lyrids, η-Aquariids, α-Capricornids, Southern δ-Aquariids, Perseids, Orionids, Southern and Northern Taurids, Leonids and Geminids. Though they are active showers, many important differences are found: dividing a meteor shower into pieces or swallowing minor showers into a major one. The differences are caused mainly by the shower definition of each system and not so much by observational devices, though some are affected by observational conditions: weather and missing the maximum. It becomes clear that there should be objective regulation especially for the finding of a new meteor shower.

Received 2018 June 6

1 Introduction

Visual, photographic, radar and video observations have shown us different appearances of meteor shower activities. Some meteor showers cannot be detectable by optical observations even at night time and others not by radar observations. Koseki gave such examples in WGN (Koseki, 2016). Now, video observations have become one of the most powerful techniques in meteor observations. But their results are widely different and even contradictory to each other in some cases. Do the differences in video observations come from the variety of devices or capturing software? The SonotaCo network (SonotaCo, 2017) and CAMS (Jenniskens et al., 2016) are reservoirs of individual meteor data and give chances to investigate the causes of the differences. We study the problem through SonotaCo's data and CAMS's.

2 Overview on the differences in devices and observability

Japanese meteor enthusiasts tried to use surveillance cameras (CCTV) in the 2000's and soon they noticed a bright and short focus lens can catch more meteors than a longer focus one. They have continued to use such lenses, for example: Watec WAT-100N, $f = 6$ mm $F/0.8$. CAMS started its operation in 2010 and the devices are standardized as documented in Roggemans (2015). A CAMS camera can observe a field of view of 22.5 by 29.9 degrees, while a camera commonly used in Japan has a field of view of 56 by 43 degrees. The SonotaCo net published meteor data on the Web for 2007–2016 (SonotaCo, 2017). The calculations and surveys can be easily carried out by any individual observer/researcher, while CAMS data are analyzed in a centralized procedure.

CAMS data are now available only from 2010 October 21 to 2013 March 29 (Jenniskens et al., 2016). We therefore limited the use of SonotaCo data to 2010–13 and CAMS data 2011 January to 2012 December and, therefore, amounts of each data set are nearly equal.

[1]The Nippon Meteor Society, 4-3-5 Annaka-shi, Gunma-ken, 379-0116, Japan. Email: geh04301@nifty.ne.jp

IMO bibcode WGN-464-koseki-definitions
NASA-ADS bibcode 2018JIMO...46..119K

2.1 Focal length and magnitude distribution

CAMS uses a larger lens and, therefore, can detect fainter meteors than the optics used by the SonotaCo network. Figure 1 shows clearly our expectation: meteor numbers of SonotaCo net fall more quickly for meteors fainter than 1st magnitude. But, it shows that CAMS caught bolides more often than what we expect from the magnitude distribution curve itself. The SonotaCo distribution curve declines more steeply for brighter meteors than CAMS. It is suggested that the magnitude measurement method is different in the two systems.

The author pointed out that the CCD observations (SonotaCo net) catch fewer meteors with a slow geocentric velocity than fast ones (Koseki, 2015). Figure 2 shows the comparison between the CAMS and the SonotaCo net meteors concerning velocity distribution. The main peak of SonotaCo net concerns the Geminids, the second is the Apex source including the Orionids and the third are the Perseids. Though hyperbolic meteors ($V_g > 74$ km/s) are recorded more often in CAMS than in the SonotaCo net, the latter got more meteors over 50 km/s. CAMS can catch about twice as many slow meteors ($V_g < 20$ km/s) than the SonotaCo net, although photographic observations recorded much more slow meteors than CAMS.

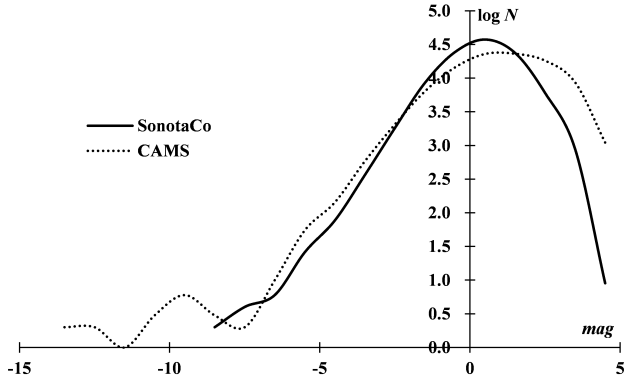

Figure 1 – Magnitude distribution: x-axis is video magnitude and y-axis is logarithmic number of meteors.

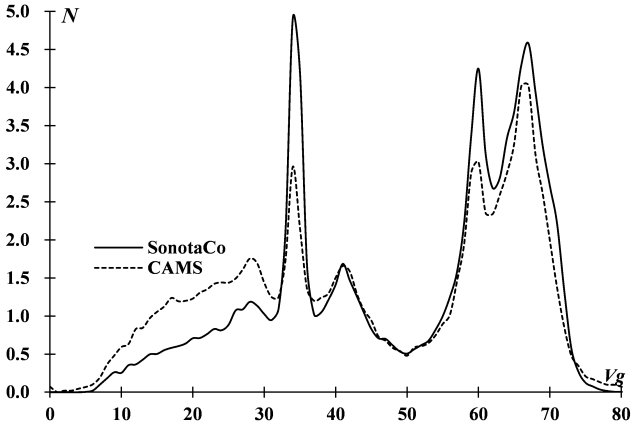

Figure 2 – Velocity (km/s) distribution standardized by the total number of meteors.

2.2 Focal length and velocity distribution

We can see the difference in the observability in velocity by comparing the moving mean magnitude (binned per thousand meteors) as a function of the velocity (Figure 3). It is clear that CAMS can detect more faint meteors than SonotaCo over the whole range and the difference becomes larger for slower meteors. A shorter focal length camera records a meteor trail shorter than a longer focal length lens such as used by CAMS. Fainter and shorter meteor trails might be rejected as noise in the SonotaCo net.

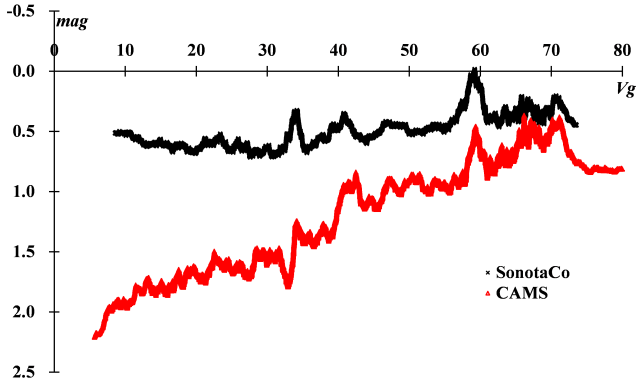

Figure 3 – Moving mean magnitude (bins of a thousand meteors) against velocity (km/s).

3 Statistical results

3.1 Accuracy of the data

Perseids and Geminids are the representative meteor showers of fast and medium velocity and their data are massive enough to compare two data sets. According to the respective shower definitions of both SonotaCo and CAMS, we use meteors for Perseids (PER) of $\lambda_\odot = 135 \sim 145$ and Geminids (GEM) $\lambda_\odot = 255 \sim 265$. We often use IAUMDC 3 character codes (IAUMDC, 2018) to shorten shower names and give a quick reference table in the Appendix. Figure 4a (PER) and 5a (GEM) show the radiant density per square degree from each radiant centered at PER $(\lambda - \lambda_\odot, \beta) = (283.2, 38.5)$ and GEM $(\lambda - \lambda_\odot, \beta) = (208.1, 10.5)$. Total numbers of PER and

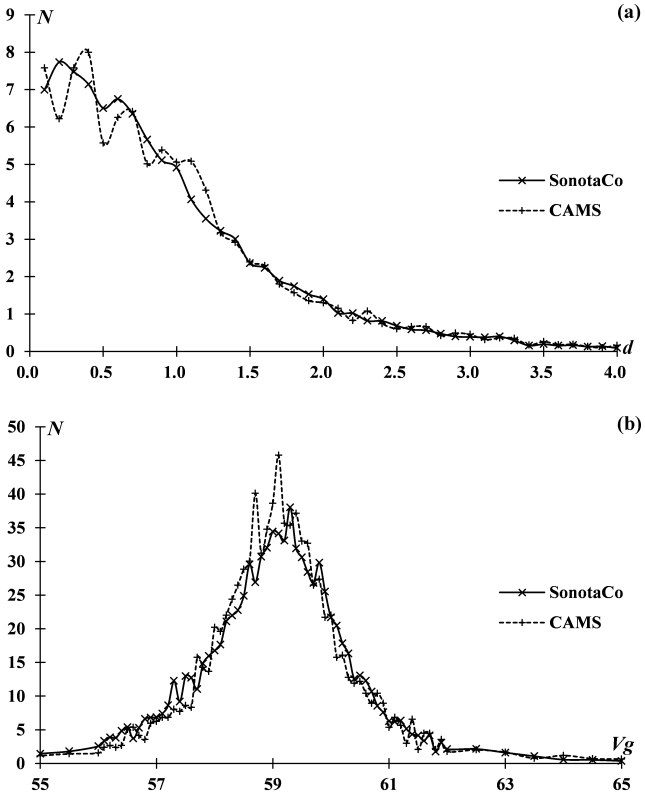

Figure 4 – Comparison between SonotaCo and CAMS in Perseids. (a): the distribution of the radiant density (N/square degree) with the distance (d; degrees) from the mean radiant in $(\lambda - \lambda_\odot, \beta)$ coordinates, (b): the velocity (km/s) distribution. Both distributions are standardized by the total number of meteors.

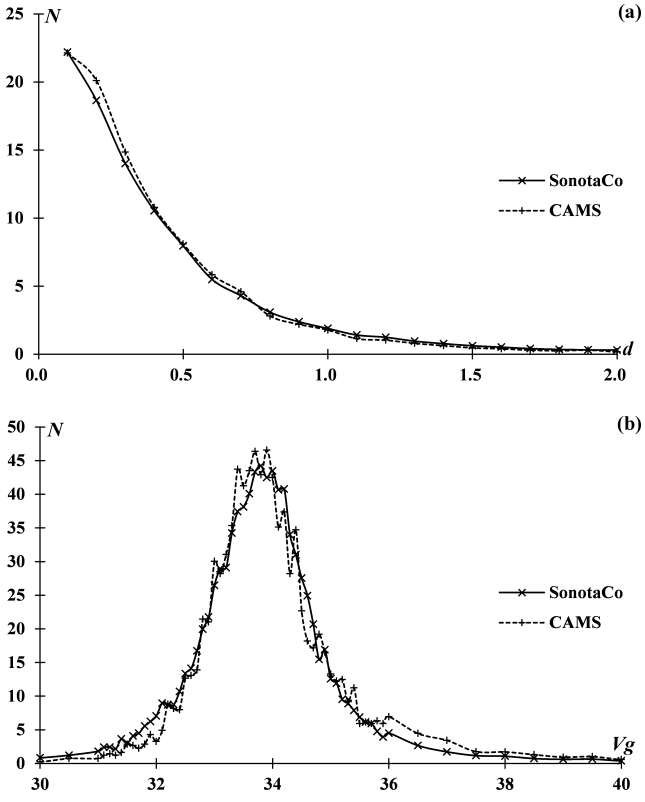

Figure 5 – Comparison in Geminids. Explanatory notes are the same as Figure 4.

GEM are different in the two data sets and, therefore, it is necessary to compensate by cumulative density in total. Both curves bear a striking resemblance and it is clear SonotaCo net and CAMS determined radiants accurately for medium and fast showers. Figure 4b and 5b show the velocity distribution (again, standardized by the total number) and clear coincidence as in the case of the radiants.

We can confirm the accuracy by the statistics of PER and GEM (Table 1a and Table 1b). Each statistic has two lines, upper for CAMS and lower for SonotaCo net. The two systems give a very similar mean/median and the standard deviations and tables may suggest that SonotaCo data are rather better than CAMS. Further, you may notice the curious minimum and maximum radiant data $(\lambda - \lambda_\odot, \beta)$ for CAMS (Table 1b). There are some clearly misplaced meteors among the Geminids and 9 meteors which belong to σ-Hydrids (HYD) should be excluded also. It seems there is some error in the search software of CAMS.

3.2 Shower members and sporadics

Table 2 (full shower names and their principal data are given in the Appendix) shows meteor shower ranking by SonotaCo net and CAMS comparing with the representative radar observations CMOR2 (Brown et al., 2010). The values of each source in Table 2 are standardized number by setting the first shower to 10, because total meteor numbers in the three data sets, especially CMOR2, are different. CMOR2 naturally includes daytime showers, indicated by asterisks and, if we excluded them from the list, we could add 7 showers: 1.98(*NID*), 1.95(PER), 1.85(NOO), 1.82(NIA), 1.81(*PCA*), 1.78(CTA), 1.63(NZC). _S26 in the SonotaCo net row is not an IAUMDC code but indicates Sirko's shower No.26 (Molau, 2010).

We recognize easily the difference between the two video observations as against radar ones. CMOR2 caught abundant toroidal meteors (italic names denote members of such group). It is noticeable that PER is lost in CMOR2 and QUA comes second. PER has commonly been detected only as weak activity by radar observations (for an example, see Sekanina, 1970). CMOR placed QUA as one of the toroidal group and includes broad activities around its area.

Table 3 (for 3 character codes, see Appendix) shows the percentages of the recorded meteors in the classical meteor showers numbered in the IAUMDC list within No.31. Zeroes in Table 3 have different meanings; 0 is no definition in their shower definition table and 0.00 is no meteors or very small number found. You may doubt that NDA is not detected in SonotaCo net, but SonotaCo net uses the code 'BPI' originally for NDA and 'NDA' in SonotaCo net is used as the classical definition (Wright et al., 1957).

We see both video observations look alike compared to CMOR2; the first to third showers are the same. But Table 3 reveals the percentage of GEM in SonotaCo net is double CAMS's. We notice several SonotaCo net showers contain larger meteor numbers than CAMS: STA double, LEO six times, HYD triple, NTA triple, COM quadruple. There are a few showers where the opposite is true; CAP and SDA are half. SonotaCo net aims to define wider shower radiant areas and classify neighbor meteors as shower members; percentages of many showers in SonotaCo net exceed CAMS's and sporadics of SonotaCo net are less than CAMS by over 10%.

4 Differences in meteor showers

We find α Draconids (DAD) is 12$^{\text{th}}$ in the SonotaCo net list in Table 2, though it is only a minor weak shower in CAMS. We meet many differences in the two data sets, though the ability of the two networks is almost equal as shown above. What is the cause of such differences? There may be several factors; shower definition, weather conditions, chance to encounter the true maximum, etc. We will research the problem in the following sections individually.

4.1 Quadrantids (QUA) and December α Draconids (DAD)

Quadrantids have been thought as a unique meteoroid shower that has an orbit almost perpendicular to the ecliptic plane. However, Brown et al. (2010) placed it as one of the Toroidal members and recent radar and video observations have revealed there are many small activities around the Quadrantids. December α Draconids (DAD) are an example and affect the Quadrantid observations of SonotaCo net.

SonotaCo net defines DAD as RA = 207.9, Dec. = 60.6, peak $\lambda_\odot = 256.5$, $\Delta\alpha = 0.40$, $\Delta\delta = -0.14$ and, which is worse, radiant radius R=9.0 degrees (SonotaCo, 2009). Therefore, SonotaCo net classifies some

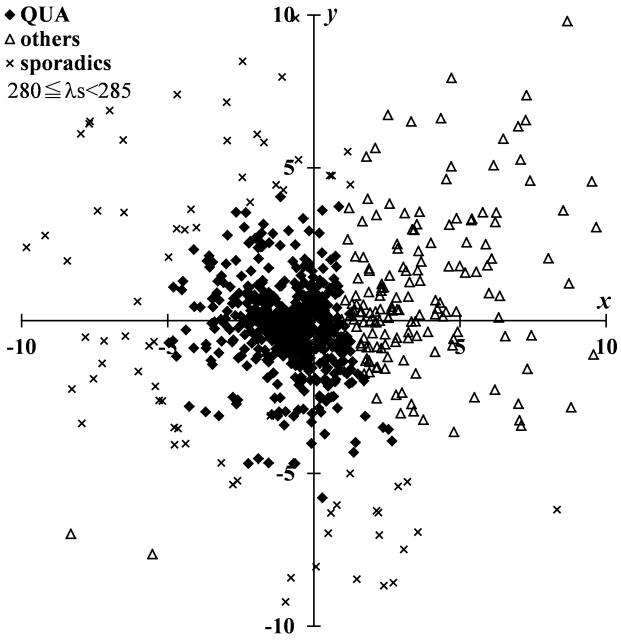

Figure 6 – SonotaCo radiant distributions: azimuthal equidistant projection in ecliptic coordinates centered at $(\lambda - \lambda_\odot, \beta) = (277, 64)$. The line $\lambda - \lambda_\odot = 277$ runs along y-axis. Intervals on axes marked in degrees and $\lambda - \lambda_\odot$ increases to the left. All meteors in solar longitude range 280 to 285 are plotted. Quadrantids are eroded by December α Draconids (DAD) in SonotaCo net observations.

Table 1a – Perseids; the first line for each statistic shows the values for CAMS and the second line the values for SonotaCo net. Data are listed for radiant in ecliptic coordinates, solar longitude, beginning and end heights, peak video magnitude along the meteor trail, geocentric velocity and the usual orbital elements.

	$\lambda-\lambda_\odot$	β	$\lambda_\odot$	$H_{\rm beg}$	$H_{\rm end}$	Mv	V_g	e	q	i	ω	Ω	$1/a$
Min	275.9	29.5	116.0	89.4	65.8	−6.5	53.4	0.609	0.819	97.9	126.8	116.0	−3.265
	274.0	30.6	109.8	57.1	45.7	−7.3	34.6	0.187	0.360	82.1	18.0	109.8	−0.909
Max	292.2	47.3	157.2	142.7	115.8	4.7	84.8	4.070	1.002	128.9	167.9	157.2	0.411
	292.5	43.3	170.2	160.8	133.1	3.6	69.8	1.817	1.003	128.1	171.8	170.2	1.407
Mean	283.4	38.6	137.9	111.5	97.6	0.3	59.5	0.993	0.947	113.1	150.3	137.9	0.009
	283.1	38.4	138.2	108.3	93.5	−0.2	59.0	0.948	0.947	113.0	149.9	138.2	0.058
SD	1.85	1.77	5.54	4.04	4.79	1.52	2.40	0.218	0.020	2.98	4.99	5.54	0.226
	1.83	1.53	5.73	4.15	6.07	1.12	1.98	0.123	0.031	2.89	8.22	5.73	0.143
Median	283.3	38.5	139.3	110.9	98.0	0.4	59.1	0.951	0.949	113.1	150.4	139.3	0.052
	283.0	38.5	139.3	108.2	94.4	−0.2	59.2	0.956	0.951	113.1	150.8	139.3	0.047

Table 1b – Geminids; the line order is same as Table 1a.

	$\lambda-\lambda_\odot$	β	$\lambda_\odot$	$H_{\rm beg}$	$H_{\rm end}$	Mv	V_g	e	q	i	ω	Ω	$1/a$
Min	174.3	−39.2	243.2	85.3	54.1	−6.1	6.8	0.128	0.059	4.0	0.7	81.5	−1.792
	195.8	1.0	236.0	50.8	40.5	−5.5	18.6	0.604	0.038	2.4	301.2	236.0	−0.221
Max	305.6	61.0	269.8	117.6	114.4	5.0	65.9	1.148	0.829	148.0	338.8	269.7	1.602
	217.6	17.2	289.2	189.0	173.0	3.9	48.5	1.036	0.346	55.9	340.3	289.2	1.290
Mean	208.1	10.5	261.1	97.0	85.0	1.6	34.1	0.891	0.144	23.3	324.0	261.0	0.749
	208.1	10.4	261.4	94.5	80.9	0.5	34.0	0.890	0.145	23.0	324.2	261.4	0.754
SD	2.40	1.56	2.21	2.51	4.41	1.38	1.99	0.026	0.020	4.02	8.13	4.89	0.119
	1.37	1.35	3.07	4.52	7.09	1.00	1.85	0.023	0.019	3.49	2.53	3.07	0.105
Median	208.1	10.5	261.7	97.0	85.5	1.7	33.8	0.889	0.145	22.9	324.3	261.7	0.766
	208.1	10.5	261.8	94.5	82.2	0.5	33.9	0.890	0.145	22.9	324.3	261.8	0.763

Table 2 – Major sources of meteor activity. The value for each source is the number of meteors standardized to the first ranked source as 10.

rank	SonotaCo		CAMS		CMOR2	
1	10.00	GEM	10.00	GEM	10.00	GEM
2	5.44	PER	8.76	PER	6.37	QUA
3	2.63	ORI	5.73	ORI	4.64	SDA
4	1.61	COM	2.78	SDA	3.46	ARI*
5	1.41	STA	1.88	ETA	3.43	TCB
6	1.40	HYD	1.69	STA	3.17	SMA*
7	1.14	LEO	1.28	CAP	3.15	ETA
8	1.11	NTA	1.24	QUA	2.64	LBO
9	0.99	ETA	1.12	HYD	2.52	XCB
10	0.64	SDA	0.94	NTA	2.51	APS*
11	0.62	QUA	0.93	COM	2.44	ORI
12	0.57	DAD	0.82	NZC	2.41	STA
13	0.46	NOO	0.76	PPS	2.22	ZPE*
14	0.42	SPE	0.72	NOO	2.20	NTA
15	0.41	MON	0.68	AOA	2.20	NOC*
16	0.31	CAP	0.58	NUE	2.18	LEO
17	0.27	BPI	0.57	XAR	2.13	SIA
18	0.23	LYR	0.53	NDA	2.12	OCE*
19	0.22	_S26	0.50	LYR	2.02	NDA
20	0.21	ERI	0.50	MON	1.98	DLT*

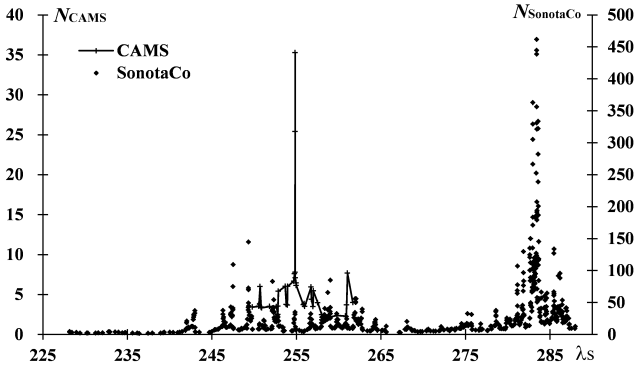

Figure 7 – Numbers of classified DAD meteors derived from span of 7 meteors, that is, $N = 7/\Delta\lambda_\odot$. Left axis is for CAMS and right SonotaCo net.

meteors having $\lambda_\odot > 265$ as DAD. Figure 6 shows SonotaCo net's DAD erodes QUA because of its definition. Figure 7 shows DAD activity by CAMS and by SonotaCo net, derived from the span of 7 meteors at a time (i.e., the estimated number of meteors in one solar longitude bin is given by $N = 7/\Delta\lambda_\odot$ where $\Delta\lambda_\odot$ is the time span of 7 meteors). It is clear meteors recorded around $\lambda_\odot = 255$ are DAD, and SonotaCo net's 'DAD' around $\lambda_\odot = 283$ are QUA.

It is unfortunate for readers who use the reported results in the IAUMDC list only, because SonotaCo net's DAD and QUA are both distorted. This is an extreme case but there might be many chaotic cases because of the activity period being heedlessly prolonged.

DAD is listed by IAUMDC as 'established' status but what is indicated by DAD is unclear now. Figure 8 shows meteor radiants during $\lambda_\odot = 250 \sim 265$ observed by SonotaCo net 2007∼16 centered at $(\lambda-\lambda_\odot, \beta) = (266.1, 63.0)$ of SonotaCo net's DAD. December κ Draconids (DKD) on the right edge is active at the maximum of DAD and DAD is located near QUA but the

Table 3 – Percentages of meteors classified as famous meteor showers in CAMS and SonotaCo net.

IAUNo.	SonotaCo	CAMS	IAU code
1	0.36	0.64	CAP
2	1.60	0.85	STA
3	0	0	SIA
4	11.34	5.02	GEM
5	0.73	1.40	SDA
6	0.26	0.25	LYR
7	6.17	4.40	PER
8	2.98	2.87	ORI
9	0.00	0.03	DRA
10	0.70	0.62	QUA
11	0.06	0.00	EVI
12	0.14	0.03	KCG
13	1.29	0.20	LEO
14	0	0	XOR
15	0.21	0.07	URS
16	1.59	0.56	HYD
17	1.26	0.47	NTA
18	0.05	0.03	AND
19	0.47	0.25	MON
20	1.82	0.47	COM
21	0.01	0.01	AVB
22	0.08	0.06	LMI
23	0.15	0.03	EGE
24	0.00	0	PEG
25	0	0.05	NOA
26	0.00	0.26	NDA
27	0.01	0.02	KSE
28	0	0.15	SOA
29	0	0	DLE
30	0	0	PSC
31	1.12	0.95	ETA
	6.82	8.59	others
	60.76	71.71	sporadics

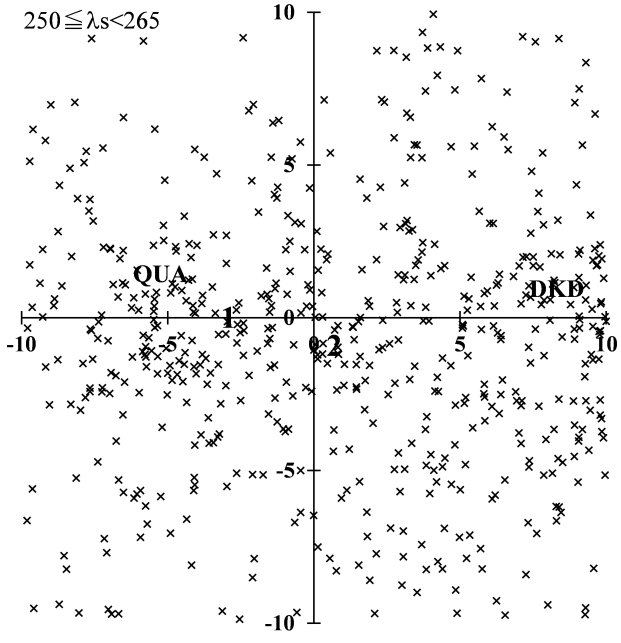

Figure 8 – Radiant distribution recorded by SonotaCo net 2007∼16 centered at $(\lambda - \lambda_\odot, \beta) = (266.1, 63.0)$. Details in the text.

maximum of QUA occurs after the end of DAD activity by two weeks. Numerals 1 and 2 indicate CAMS's observations of DAD's AdNo 1 and 2 (AdNo is an additional number given by IAUMDC for each entry, to distinguish different entries for the same shower). Ten years observations cannot specify the center of DAD; small concentrations might be pointed out around 1, 2 and QUA or below QUA. CAMS overlaps one of the toroidal showers detected by CMOR, namely the November i Draconids (NID), with DAD and classifies more meteors as NID than DAD, though NID is a working status shower. Meteors around the center of this figure might be classified as either NID or DAD depending on the definition of a researcher.

4.2 April Lyrids (LYR)

The Lyrid shower is so distinctive that we can separate it from background activities almost completely, because the profile of the activity is sharp and there are poor sporadic radiants around its position. Comparison/identification between different observations can give good results in case of these two conditions being fulfilled. Figure 9 shows the profiles of Lyrids giving recorded numbers of meteors in each 1 degree bin. Both profiles of CAMS and SonotaCo net are alike and exhibit a narrow activity period. But it is interesting to note that the Lyrids' activity fluctuates sometimes.

Recorded meteor numbers are affected by weather conditions of course, but the difference between observational time and the above mentioned narrow maxi-

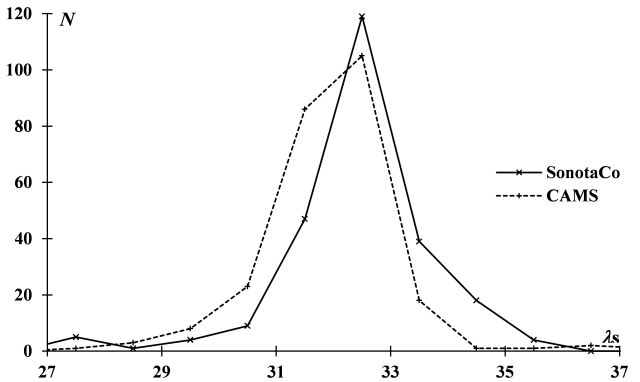

Figure 9 – Lyrid activity in general view: SonotaCo (2010∼13), CAMS (2011∼12).

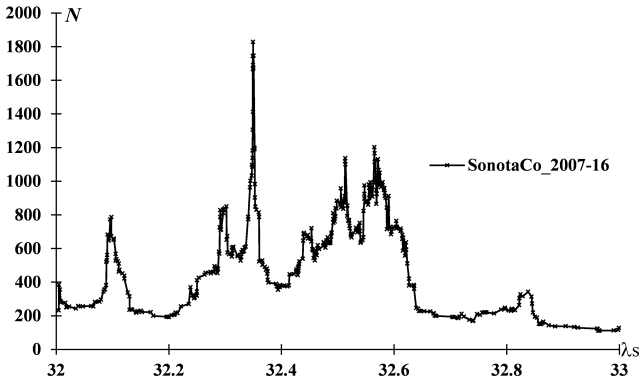

Figure 10 – Lyrids 2007∼16 activity by SonotaCo net in detail, derived from 21 meteors span, that is, $N = 21/\Delta\lambda_\odot$.

Table 4 – Lyrid meteors recorded during 2007–16 by SonotaCo net.

Code	2007	2008	2009	2010	2011	2012	2013	2014	2015	2016	Mean	SD	r(max/min)
LYR	6	73	96	37	44	14	172	152	132	45	77.1	55.5	28.7

Table 5 – Statistics of Lyrids; the line order is same as Table 1a.

	$\lambda-\lambda_\odot$	β	$\lambda_\odot$	$H_{\rm beg}$	$H_{\rm end}$	Mv	V_g	e	q	i	ω	Ω	$1/a$
Min	208.4	−12.5	21.0	91.4	71.7	−5.0	40.6	0.773	0.098	48.5	144.8	21.0	−0.240
	229.4	46.6	14.4	89.4	71.4	−2.9	37.7	0.566	0.825	66.5	203.7	14.4	−0.456
Max	251.5	64.0	44.5	136.5	104.4	3.8	50.5	1.218	0.969	85.9	223.7	207.5	0.247
	250.9	60.6	51.0	117.0	101.4	2.9	53.7	1.406	0.962	96.7	233.2	51.0	0.498
Mean	240.9	56.8	32.2	108.0	92.4	1.3	46.6	0.959	0.919	79.0	213.4	32.9	0.045
	240.9	56.5	32.4	104.6	89.3	0.2	46.8	0.958	0.917	79.7	214.8	32.4	0.046
SD	3.82	4.58	2.05	4.70	5.37	1.49	1.47	0.081	0.054	3.18	5.52	11.10	0.088
	2.88	1.68	3.92	4.00	6.11	1.09	1.90	0.101	0.017	3.11	3.94	3.92	0.112
Median	241.0	56.8	32.3	107.3	93.2	1.5	46.7	0.957	0.922	79.4	214.0	32.3	0.047
	240.9	56.6	32.5	104.7	90.0	0.3	46.9	0.958	0.919	79.7	214.4	32.5	0.046

mum also. Figure 10 shows Lyrid activity during 2007–16 (SonotaCo net) detailed profile with the estimated meteor number in one solar longitude bin given by $N = 21/\Delta\lambda_\odot$ ($\Delta\lambda_\odot$ is the time span of 21 meteors). The average maximum is $\lambda_\odot = 32.565$, corresponding to a time observable from Japan in 2013. Japanese observers recorded many Lyrids also in 2014 (Table 4). This was caused by a sudden enhancement at $\lambda_\odot = 32.350$; 20 Lyrids were captured during only 24 minutes (2014 April 22, $18^{\rm h}24^{\rm m}18^{\rm s} - 18^{\rm h}48^{\rm m}10^{\rm s}$ UT). Short lived enhanced Lyrid activities have been reported several times, for example Komaki recorded visually 103 Lyrids during 1945 April 21 $18^{\rm h}00^{\rm m} - 19^{\rm h}07^{\rm m}$ UT (Komaki, 1945); this corresponds to $\lambda_\odot = 32.052$ (J2000.0). Such phenomena could not be noticed by powerful but short term observations.

Table 5 shows the statistics of Lyrids. Mean and Median both agree well but Minimum (Min) of β are very different. CAMS's classifications are sometimes problematic as shown in section 3.1 above and include sporadics or members of other showers as the corresponding shower. CAMS and SonotaCo net apply different shower definitions for every meteor shower and we notice SonotaCo net widens the Lyrids activity period. We will see the problems of the different definitions in the following sections.

4.3 η-Aquariids (ETA)

The η-Aquariids were detected by radar as a daytime shower but video observations catch many η-Aquariids every year. SonotaCo net and CAMS get similar results (Figure 11), though the η-Aquariids were active in 2013 and the peak of SonotaCo net is therefore higher than CAMS.

Those of us observing in the northern hemisphere can observe η-Aquariids only a few hours before dawn and, therefore, the detailed profile displays a comb like structure (Figure 12). Figure 12 shows rates estimated by the time span of 11 meteors (cf. Lyrid profile, Figure 10) in CAMS 2011–12 observations. If we drew a similar detailed profile using SonotaCo net 2007–16 observations, it could not show a smooth profile but would appear comb like as CAMS does. Video observations are strong tools for meteor observations but there exists the limitation for helion sources.

A small difference between SonotaCo net and CAMS is the treatment of the late η-Aquariid activity. CAMS defines several meteors in Figure 13a as η-Aquariids and some as sporadics, but CAMS judges the activity after $\lambda_\odot = 65$ as June θ-Piscids (JTP, triangles in Figure 13b). Double circles in both figures are the estimated points by linear regression of $\lambda - \lambda_\odot$ and β as functions of $\lambda_\odot$ based on all η-Aquariids of CAMS. SonotaCo net classified such activities as late η-Aquariids.

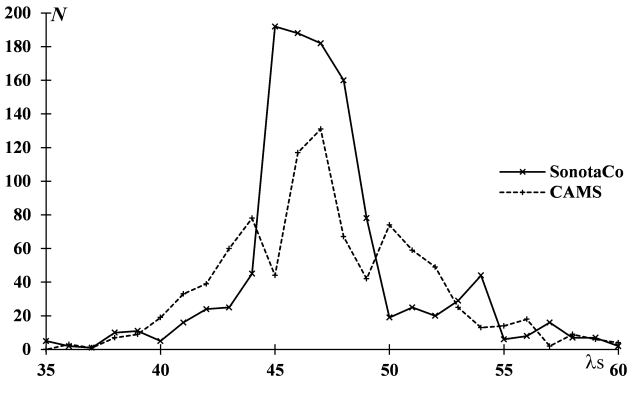

Figure 11 – η-Aquariid activity in general view.

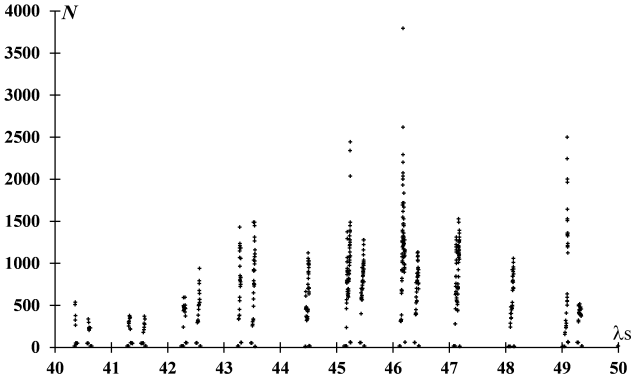

Figure 12 – η-Aquariids 2011∼12 activity by CAMS in detail, derived from 11 meteors span, that is, $N = 11/\Delta\lambda_\odot$.

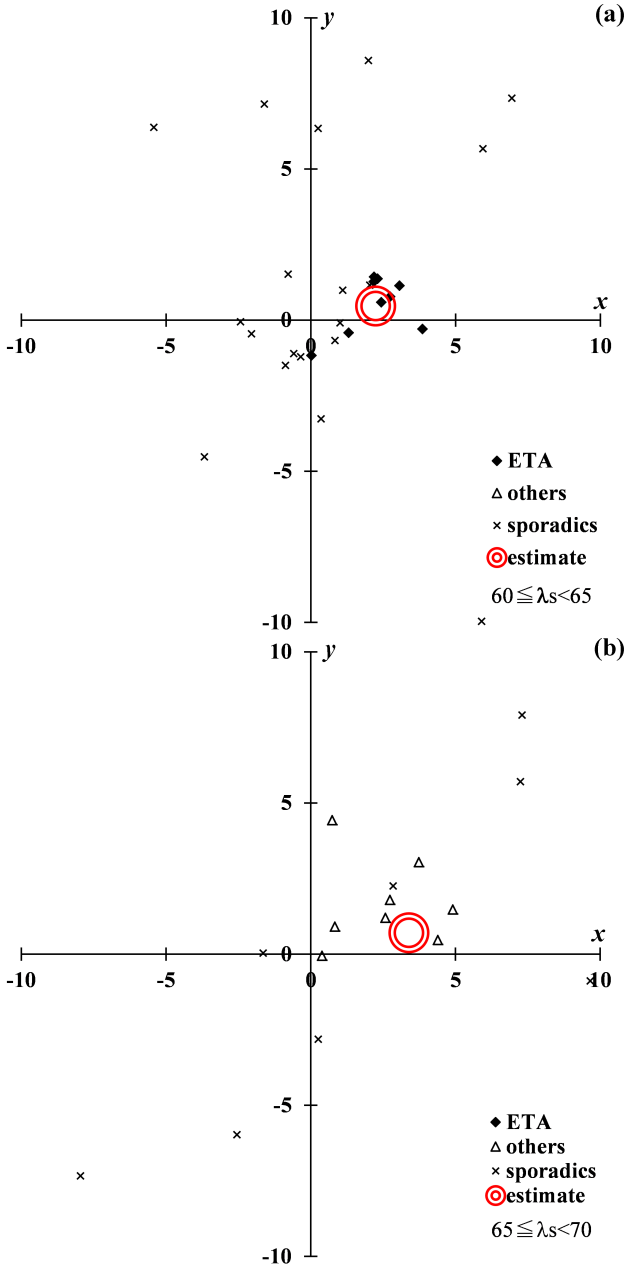

Figure 13 – Radiant distributions centered at $(\lambda - \lambda_\odot, \beta) = (292, 8)$. a: $\lambda_\odot = 60 \sim 65$, b: $\lambda_\odot = 65 \sim 70$.

4.4 α Capricornids (CAP)

The recorded number of meteors does not always express the true activity profile. Japanese weather in June to July is the worst season for optical astronomical observations and early Capricornid observations are obstructed heavily. Figure 14 shows the meteor rates by SonotaCo net and by CAMS, and SonotaCo net's rates are reduced in appearance by the weather conditions. If we use the raw data as shown Figure 14, we might be misled. One would say the Capricornid peak is at $\lambda_\odot = 129$ and another at $\lambda_\odot = 132$. If we compensate the weather conditions by using the ratios of Capricornid meteors to other meteors, both observations show the peak at $\lambda_\odot = 129$ in good agreement. The corrected figure is not given here, because the effect of the compensation will be shown in section 4.5 below and the correction does not have an influence on this following point.

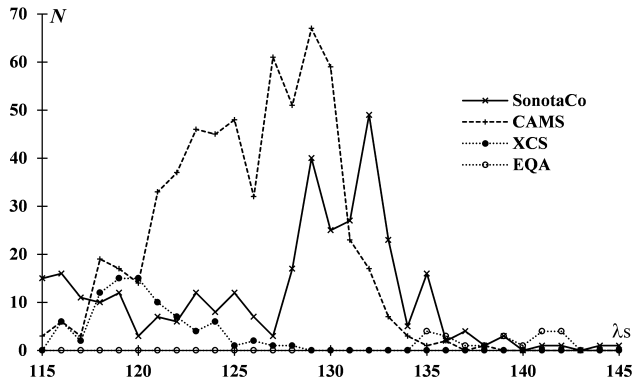

Figure 14 – α-Capricornids activity with some related showers.

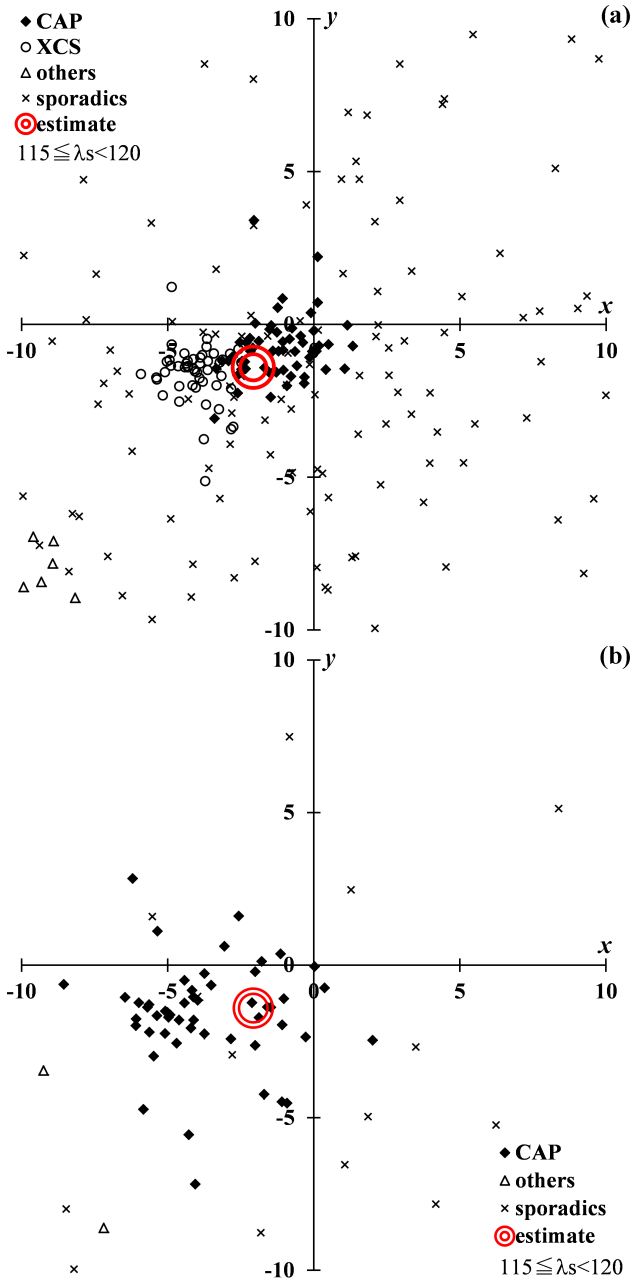

Figure 15 – Radiant distributions centered at $(\lambda - \lambda_\odot, \beta) = (180, 10)$ for meteors observed in the range $\lambda_\odot = 115 \sim 120$. a: CAMS, b: SonotaCo net.

CAMS proposes a new meteor shower called ξ2-Capricornids (XCS) in the close vicinity of CAP (Fig-

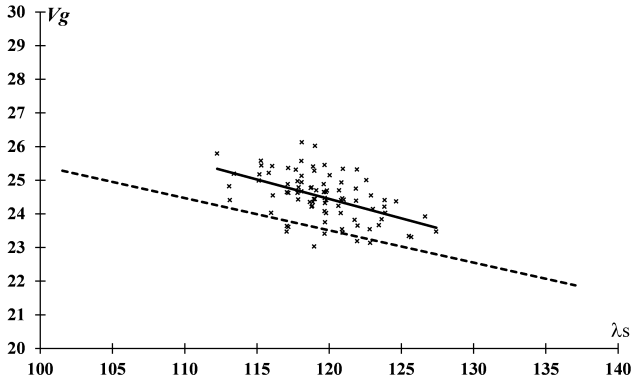

Figure 16 – Velocity distribution of XCS with the least squares solutions for XCS and CAP (dashed line).

ure 15a). CAP meteors are black diamonds and XCS triangles in Figure 15a with estimated radiant of CAP allowing for its radiant drift a double circle in Figure 15a. The estimated radiant is based on CAMS's CAP radiant only from $\lambda_\odot = 122$ to 132 and seems to be located close to the middle point of CAP and XCS at $\lambda_\odot = 115 \sim 120$. SonotaCo net observations show a slightly different view (Figure 15b) and there might be a gap between CAP and XCS. The estimated radiant is located towards the right side of the radiant group and it seems to be consistent with CAMS' CAP. Another group in the radiant plot of SonotaCo net is more active than the former and suggests the XCS activity. Figure 16 shows the velocity distribution of XCS with the least squares solutions for XCS and CAP (dashed line). XCS meteors are a little bit faster than CAPs by about 1 km/s (Figure 16).

SonotaCo net observations recorded fewer meteors than CAMS overall in this radiant area in this solar longitude range but much fewer sporadic meteors and much fewer than the CAP of CAMS (Figure 15a and 15b). This effect might be caused by the lower sensitivity of SonotaCo net to lower velocity meteors.

4.5 Southern δ-Aquariids (SDA)

As we see in section 4.4, Japanese observations are hindered by bad weather in July and the recorded number of SDA in Japan is less than CAMS (Figure 17a). We calculate the ratio of meteors within 3 degrees from radiant point (RP) to meteors 3 to 10 degrees from RP in order to compensate the weather influence. This idea is based on two assumptions: first, we could count meteors radiating within 3 degrees from RP and radiating from the outer area (3 to 10 degrees) at the same ratio when we observe them under different weather conditions. Second, we can avoid the contamination from nearby active meteor showers by setting the outer area as 3 to 10 degrees. If we use the estimated radiant as RP (see below) and count radiants within 3 degrees from RP as SDA, the corrected activity would be shown in Figure 17b. If we use the CAMS's original classification of SDA, the activity could be shown in Figure 17b as the bold line. We notice, then, that the bold line drops before $\lambda_\odot = 135$, though both activities obtained by the estimated RP (dashed lines) descend slowly.

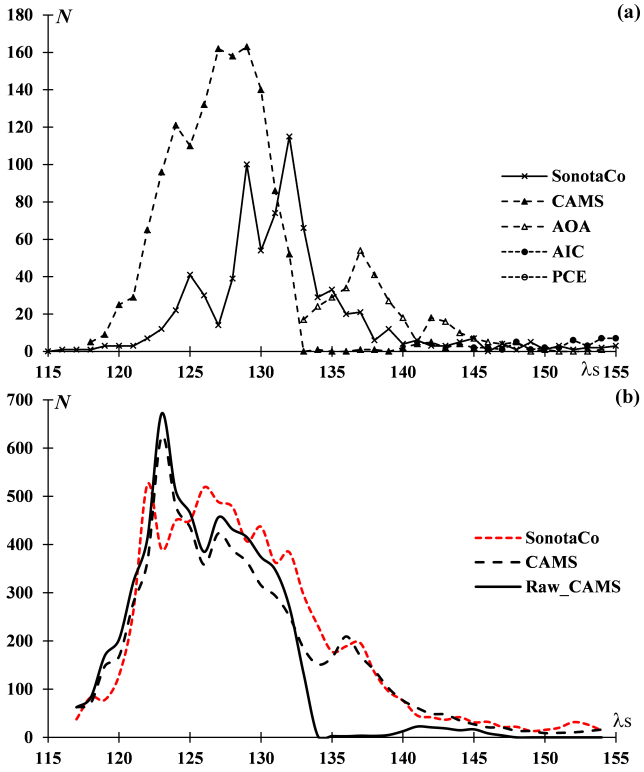

Figure 17 – Southern δ-Aquariid activity. a: raw data with some related activities, b: recounted SDA's rates to background ('Raw_CAMS' shows ratios of numbers classified as SDA originally).

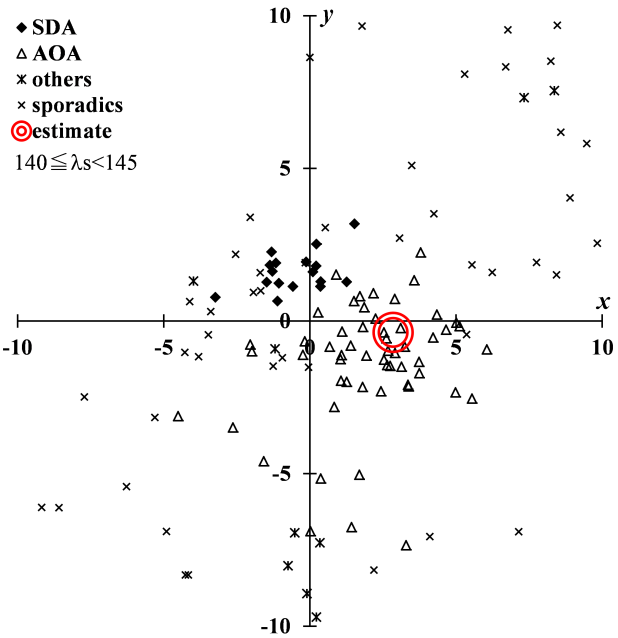

Figure 18 – Radiant distribution of late SDA and AOA centered at $(\lambda - \lambda_\odot, \beta) = (208, -8)$.

CAMS insists SDA is followed by August o-Aquariids (AOA). But it seems very difficult to distinguish SDA and AOA. Figure 18 shows the radiant distribution of SDA (black diamonds) and AOA (triangles) around $(\lambda - \lambda_\odot, \beta) = (208, -8)$. In this figure we add the estimate point of SDA on the basis of linear regression of CAMS's SDA radiants between $\lambda_\odot = 122 \sim 132$. It is very clear the estimate point is located in the middle of CAMS's AOA.

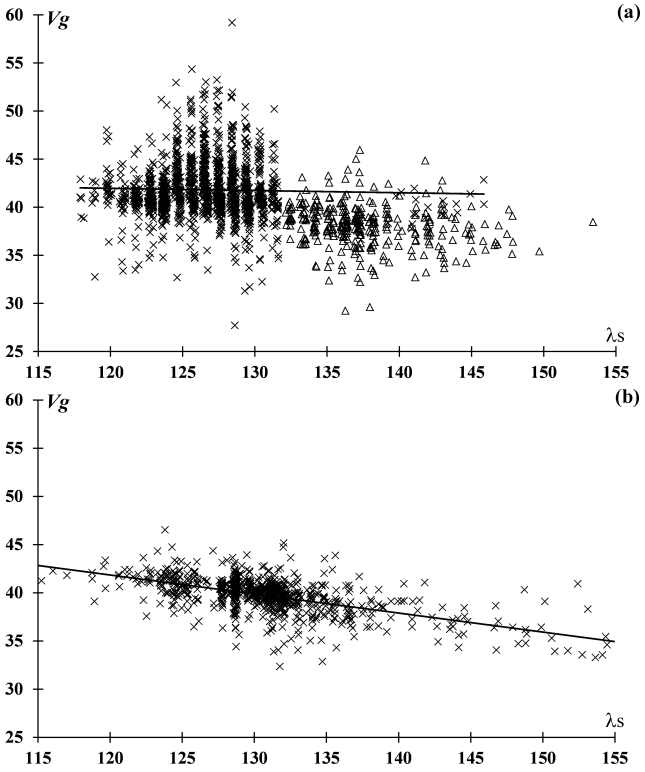

Figure 19 – Velocity distribution of SDA. a: CAMS, also showing AOA (triangles), b: SonotaCo net.

The velocity distribution of CAMS's SDA shows a wide spread (Figure 19a) and, therefore, the change with time is not clear. This could cause the confusion in the distinction between SDA and AOA. If we combined SDA with AOA, they might show similar slope with SonotaCo net results (Figure 19b). AOA is a more questionable case in the subdivision of the shower than that of CAP and XCS.

4.6 Perseids (PER)

We often intend to lengthen the activity period of a meteor shower or on the other hand to divide a meteor shower into several sections. Perseids are one of the former examples. Both SonotaCo net and CAMS recognize Perseid activity before $\lambda_\odot = 120$ and after $\lambda_\odot = 150$. Such activities seem not to be a continuous extension of the core Perseids ($\lambda_\odot = 125 \sim 145$).

Figure 20 shows the situations. The bold line expresses the extended radiant movement during $\lambda_\odot = 115 \sim 155$ estimated from CAMS's observations of the core activity. The Perseid radiant moves from upper right ($\lambda_\odot = 115$) to lower left ($\lambda_\odot = 155$) and this movement is confirmed by SonotaCo net observations also. The dashed line and dotted line represent the daily shift of the Perseid radiant for CAMS and SonotaCo net respectively; for SonotaCo net $\lambda_\odot = 119 \sim 147$ and for CAMS $\lambda_\odot = 125 \sim 149$. They are located near enough to the expected position (bold line) but the mean daily radiant departs from it before $\lambda_\odot = 125$ and after $\lambda_\odot = 145$.

CAMS's early Perseids (diamonds; $\lambda_\odot = 115 \sim 124$) are above the extreme position and SonotaCo net's (filled diamonds; $\lambda_\odot = 109 \sim 118$) far from the expected start. The bold dashed line with squares indicates radiant movement of ζ-Cassiopeiids (ZCS); the lowest square corresponds to $\lambda_\odot = 120$ and further squares upward are every $\Delta\lambda_\odot = 2.5$. It is suggested ZCS activity significantly influenced CAMS's early observations (see also SonotaCo net results of Figure 20). On the other hand, early observations of SonotaCo net might be related to 49 Andromedids (FAN).

Late radiants ($\lambda_\odot = 149 \sim 154$) in Figure 20 are distant from the bold line as with the early observations though lower right in this case; triangles for CAMS and filled triangles for SonotaCo net. There is no corresponding meteor shower in IAUMDC list. But, there might be a broad distribution of sporadic radiants (Figure 20).

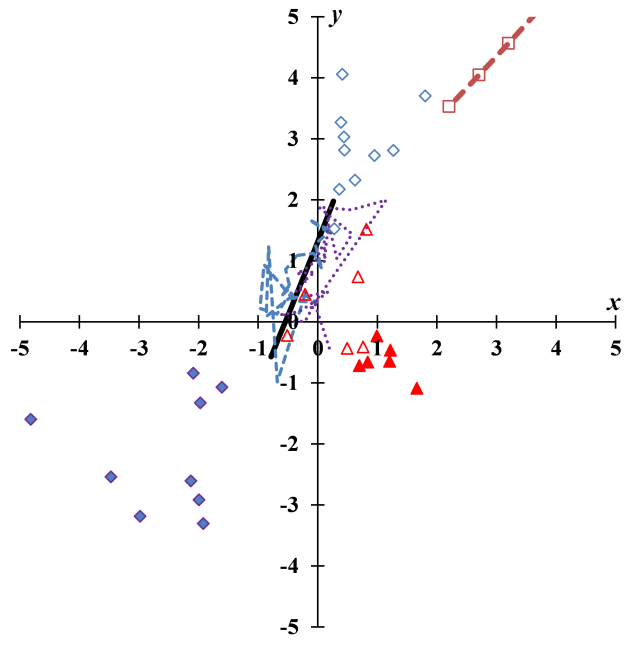

Figure 20 – Radiant drift of Perseids centered at $(\lambda - \lambda_\odot, \beta) = (283, 38)$. Details in the text.

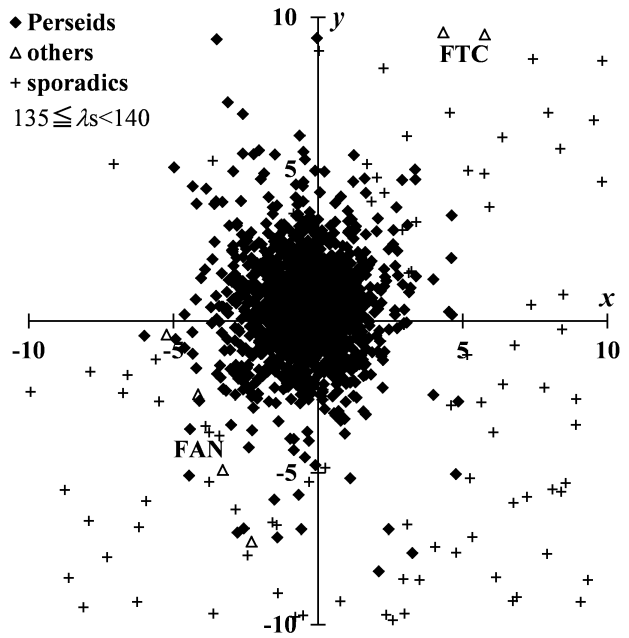

Figure 21 – Radiant distribution of Perseids by CAMS.

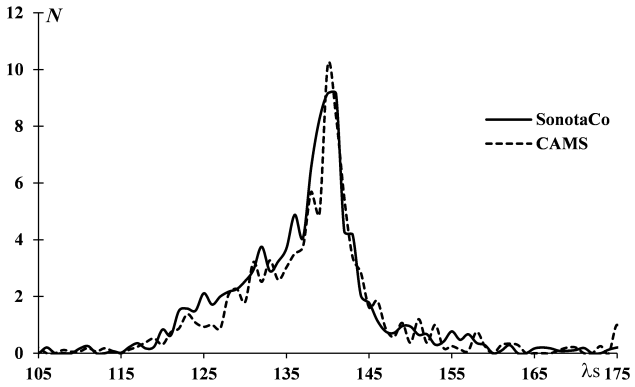

Figure 22 – Recounted Perseids, derived by calculating ratios to the background.

The Perseid radiant distribution (Figure 4a in section 3.1) and Figure 21 show Perseid radiants are located well within 3 degrees from the center. Figure 22 shows Perseid profiles drawn by the radiant ratios of meteors within 3 degrees from the estimation by CAMS as stated above to 3 $\sim$ 10 degrees, as in the case of SDA. Both CAMS and SonotaCo net results are in good agreement suggesting Perseid activity starts at $\lambda_\odot = 115$ and ends at $\lambda_\odot = 155$, though the meteors used in coming to these figures are not the same as their original classifications.

4.7 Orionids (ORI)

Orionids are another example of an overextended activity period. Both CAMS and SonotaCo net set long activity periods of Orionids in their list; CAMS $\lambda_\odot = 180.5 \sim 244.8$ and SonotaCo net $\lambda_\odot = 170.0 \sim 243.0$. But the background activities are abundant during this period in the Orionid area and the early and the late 'ORI' are questionable.

We calculate the linear regression of the radiant movement during $\lambda_\odot = 208 \sim 213$ for both CAMS and SonotaCo net data. Both these estimations are in good agreement and here we use CAMS's results. If we extend and estimate Orionid radiants before $\lambda_\odot = 208$ and after $\lambda_\odot = 213$, the estimated point could represent the observed radiant well (Figure 23b and 24a). But the radiants classified as 'ORI' have no clear concentrations around the estimated radiant before $\lambda_\odot = 190$ and after $\lambda_\odot = 230$ (Figure 23a and 24b). It is clear early Orionids are surrounded by many minor activities and sporadics (Figure 23a), though the radiant concentration of Orionids becomes significant after $\lambda_\odot = 190$ (Figure 23b). The late Orionids have close neighbor activity, comprising ZCN and sporadics also (Figure 24b), but activity around the estimated radiant is clear before $\lambda_\odot = 230$ (Figure 24a).

If we counted the radiant number within 3 degrees (d<3) from the estimated radiant, we could confirm the substantial activity period $\lambda_\odot = 190 \sim 230$ as shown above (Figure 25a). Figure 25a gives the ratio of the radiant number with d<3 to beyond 10 degrees d>10. Figure 25b shows the ratio of the number of radiants having 3<d<10 to those having d>10. The limit of 3 degrees is tight for Orionids and this condition affects

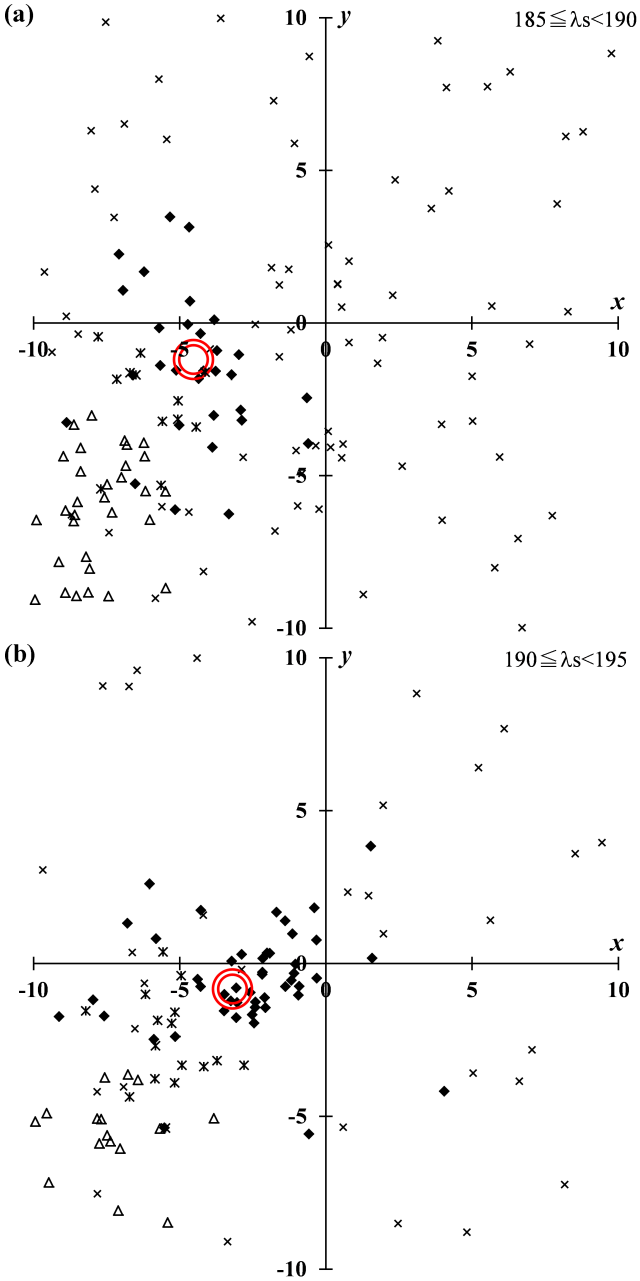

Figure 23 – Early Orionid radiant distributions centered at $(\lambda - \lambda_\odot, \beta) = (248, -8)$ by CAMS; ORI (black diamonds), ν-Eridanids (NUE; triangles), September o-Orionids (SOO; asterisks), sporadics (crosses). a: $\lambda_\odot = 185 \sim 190$, b: $\lambda_\odot = 190 \sim 195$.

the results a little: a rapid change around Orionid maximum $\lambda_\odot = 211$. But Figure 25b represents not only the influence of this tight condition around its maximum but also the long term ascending and descending profiles around Orionid maximum by the interference of neighbor activities (see Figures 23a, b and 24a, b).

4.8 Taurids (STA & NTA)

Taurids are the most distinguishable ANT (antihelion) source but the definitions of Taurids are in confusion. If we used the measure of $D_{SH} < 0.2$ (D-criterion of Southworth and Hawkins (1963)) from CAMS's own STA and NTA orbits, many minor showers would be judged as Taurids, as follows. Here we use IAUMDC Shower Code (3 letters) followed by AdNo (number 0 or

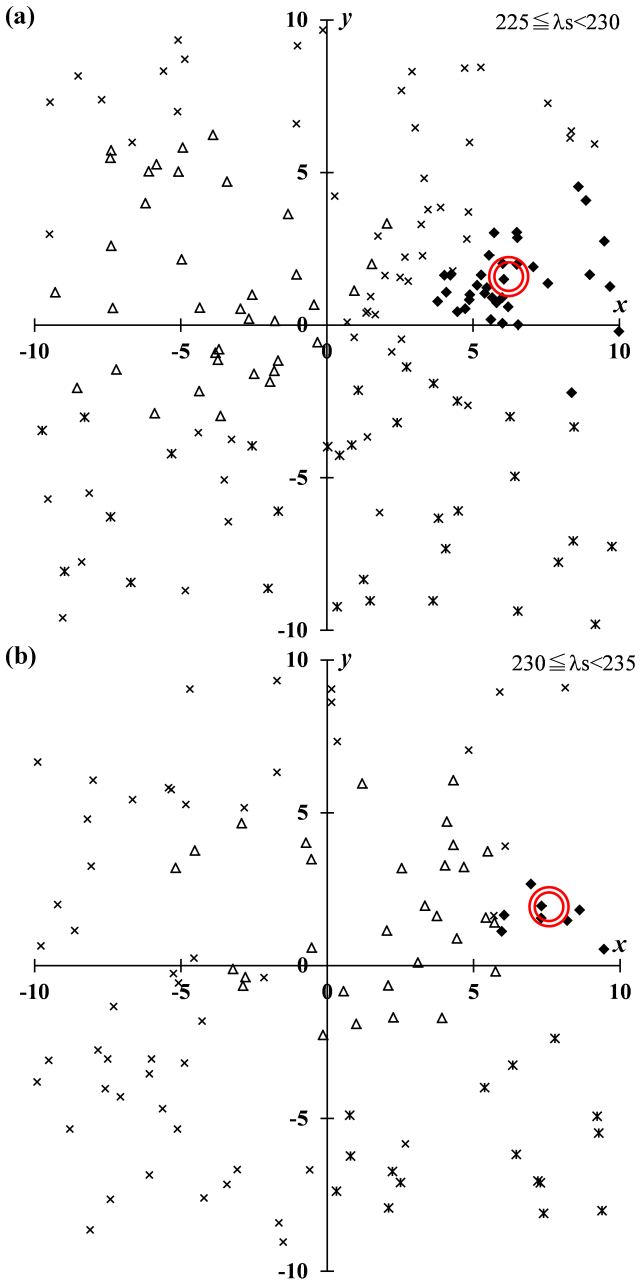

Figure 24 – Late Orionid radiant distributions centered at $(\lambda - \lambda_\odot, \beta) = (248, -8)$ by SonotaCo net; ORI (black diamonds), ζ-Cancrids (ZCN; triangles), σ-Hydrids (HYD; asterisks), sporadics (crosses). a: $\lambda_\odot = 225 \sim 230$, b: $\lambda_\odot = 230 \sim 235$.

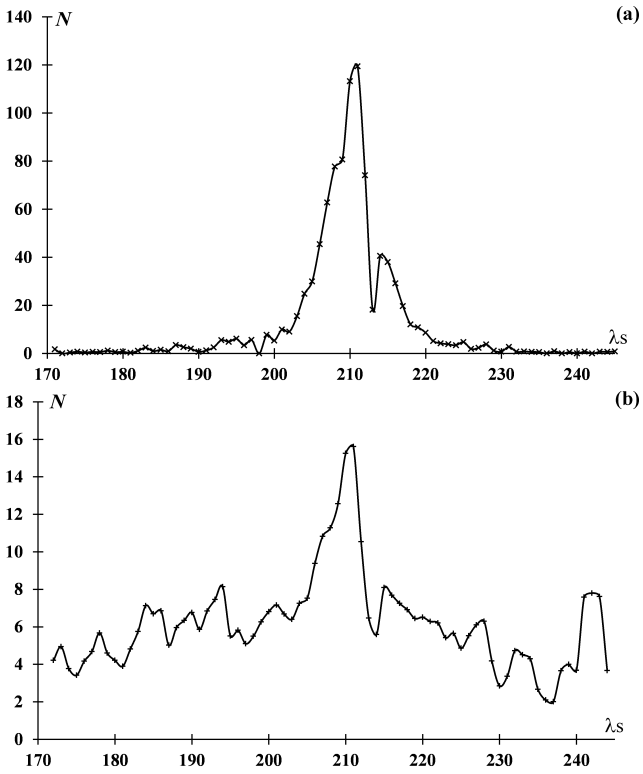

Figure 25 – Recounted radiant ratios of CAMS. a: Orionid activity (ratio d<3 to d>10), b: surrounding activity (ratio 3<d<10 to d>10).

higher) to indicate the individual record because some showers have several entries with different orbits; we also list D_{SH} in the parentheses. For STA, λ-Cetids (LCT0: 0.026), s-Taurids (STS0: 0.082), f-Taurids (FTR0: 0.087), ξ-Arietids (XAR0: 0.097), λ-Taurids (LTA0: 0.114), τ-Arietids (TAR0: 0.172), Southern October δ-Arietids (SOA1: 0.176), δ-Arietids (DAT0: 0.176), Northern October δ-Arietids (NOA1: 0.184), and for NTA, TAR0 (0.030), DAT0 (0.064), November η-Taurids (NET0: 0.090), NOA1 (0.103), A1-Taurids (ATU0: 0.108), A2-Taurids (ATS0: 0.129), FTR0 (0.145), STS0 (0.149), p-Taurids (PTS0: 0.164), LTA0 (0.168), LCT0 (0.183). Moreover, radiants of five showers overlap on Taurids; Northern δ-Piscids (NPI4), Southern δ-Piscids (SPI4), Northern χ-Orionids (ORN2), Southern χ-Orionids (ORS3), ω-Taurids (FTA1).

The Taurids are a good example of how small we can and cannot divide a meteor shower. There are many sub-streams in CAMS's list (Jenniskens et al., 2016). Figure 26a shows, for example, the radiant distribution of STA and sub-streams proposed by CAMS around $(\lambda - \lambda_\odot, \beta) = (193, -5)$ with the estimated RP of STA. We used here SonotaCo net's Taurid data between $\lambda_\odot = 210 \sim 250$ for the estimated RP, because CAMS cuts the Taurids down into pieces. The center of STA is eroded by LCT and STS and makes a hole in the STA distribution. CAMS insists there are gaps in activities and radiant positions, but the distribution of remnant STA radiants is located unnaturally.

Figure 27a represents the profiles of STA classified by each of the two data sets and it is clear CAMS's STA changes curiously not showing a clear maximum. CAMS's STA is eroded by other activities in addition to LCT and STS.

Figure 26b gives another confused situation in NTA around $(\lambda - \lambda_\odot, \beta) = (190, 3)$ with the estimated RP of NTA from SonotaCo net's Taurid data between $\lambda_\odot = 210 \sim 250$. The solar longitude period of Figure 26b is near the NTA maximum that is ordinarily recognized, but the number of CAMS's NTA radiants is only 9 in this area. The estimated radiant point is occupied by ATS and ATU.

The profile of CAMS's NTA (Figure 27b) is curious as with STA. The remnants of NTA seem to present a bimodal profile and to suggest the existence of two minor showers rather than a single major shower i.e. NTA.

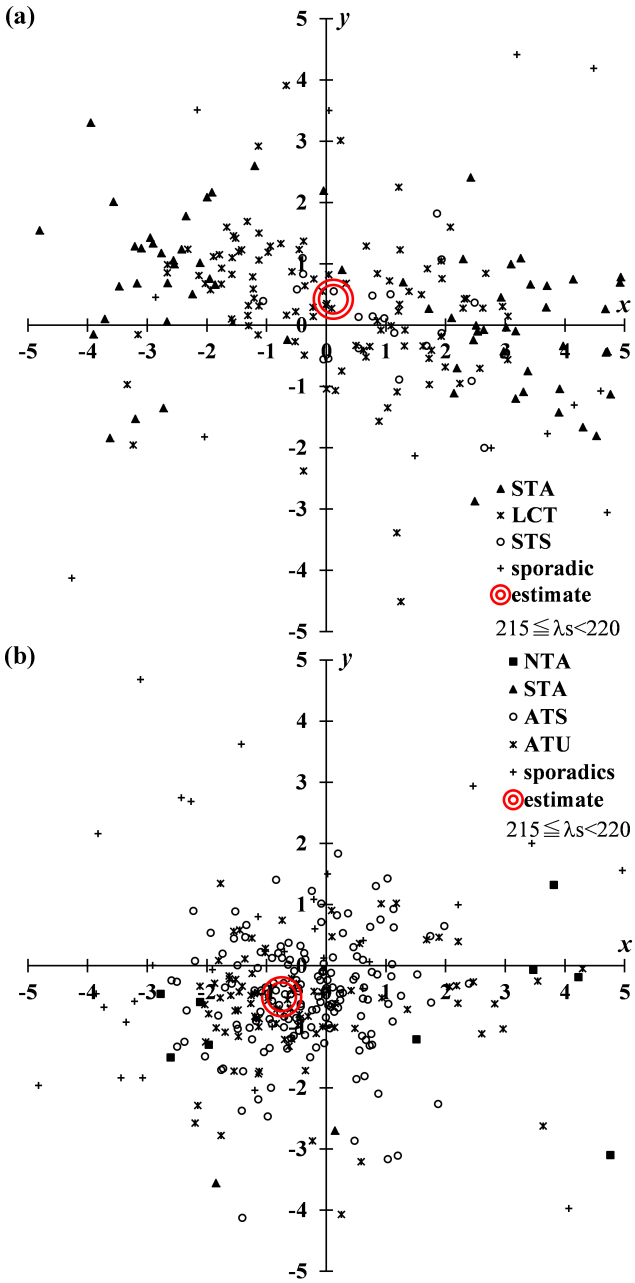

Figure 26 – Radiant distributions of CAMS. a: STA and surrounding activities centered at $(\lambda - \lambda_\odot, \beta) = (193, -5)$, b: NTA and surrounding activities centered at $(\lambda - \lambda_\odot, \beta) = (190, 3)$.

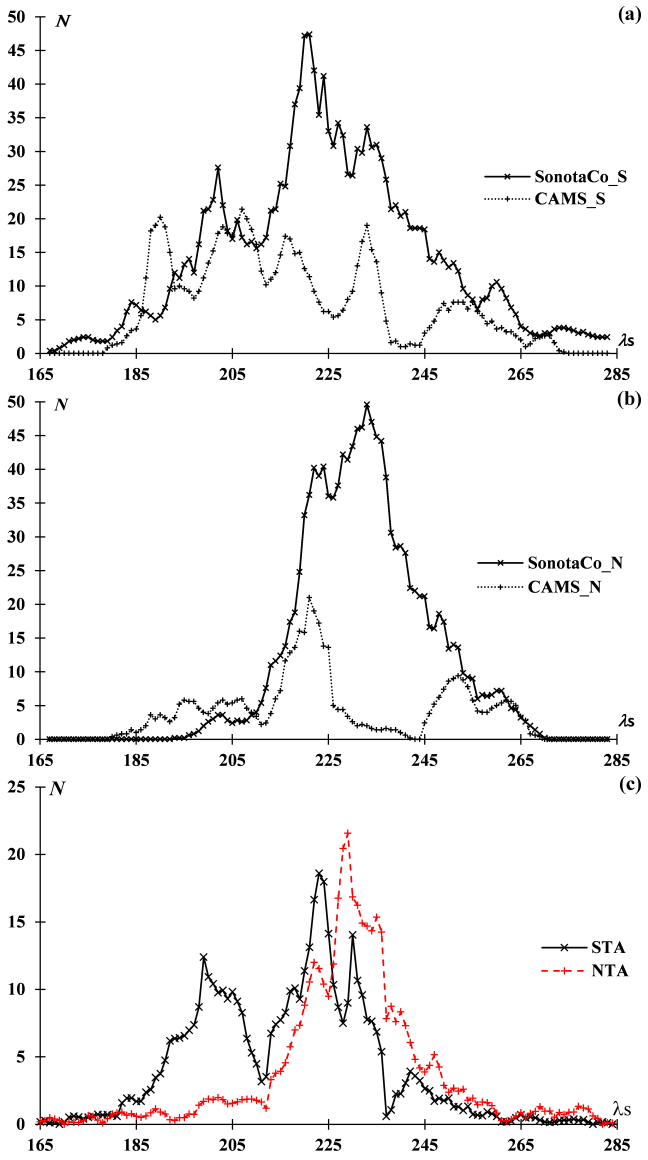

Figure 27 – Activity profiles of Taurids. a: originally classified STA, b: originally classified NTA, c: recounted radiants using ratio d<3 to d>10. a and b are the moving mean using 5 degree bins and c uses a 3 degree bin. Original counts fluctuate significantly and a and b seem to be necessary to smooth even 5 degree bins.

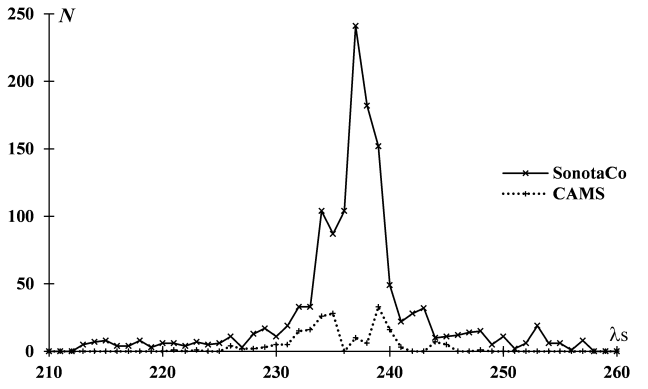

Figure 28 – Activity profile of Leonids.

If we calculated the ratio of CAMS's meteors within 3 degrees from the estimated radiants to those of the outer region as we did in Orionids, the profiles of STA and NTA (Figure 27c) would become quite similar to SonotaCo net's (Figure 27a and b). It seems inappropriate to divide Taurids into such small parts, as we have not named each dust trail individually.

The author suggested the Taurids have three components (Koseki, 2012) as Whipple did (Whipple, 1940): NTA and two STA branches. Figure 27a, b and c can uphold this idea.

4.9 Leonids (LEO)

Leonids is a clear example of where one or two years' observations might miss even a major shower. CAMS lacked observations around the very maximum of the Leonids (Figure 28). This is the reason why SonotaCo net recorded six times CAMS's Leonid meteors.

It is well known that the Leonid shower changes its nature with a 33 year period. When we describe the

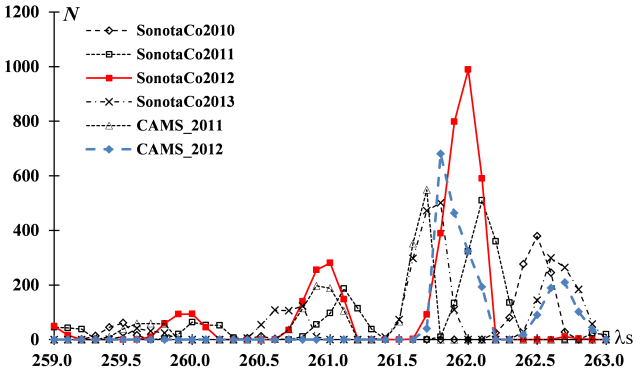

Figure 29 – Activity profile of Geminids using 0.1 degree bins.

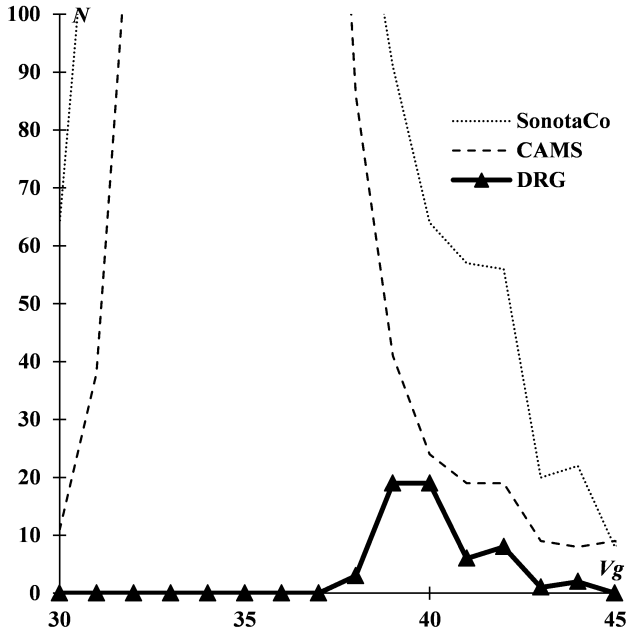

Figure 30 – Velocity distributions of GEM and DRG.

records of Leonids, it is essential to note when the observations were done.

4.10 Geminids (GEM)

We may assume that every line of data from IAUMDC informs us of a true shower maximum but real observations are affected by many conditions. Figure 29 shows recorded numbers of GEM in 0.1 degree bins and exhibits the observational limitation. SonotaCo net observers met the very maximum of GEM in 2012 and this is the reason why SonotaCo net had gotten more GEM than CAMS (see Table 3). It is clear we cannot find out the true maximum of showers by only a few years' observations.

December ρ-Geminids (DRG) are another example of how small we can or cannot divide a meteor stream. CAMS insists DRG meteors are higher velocity than GEM and distinguishable from GEM clearly (Jenniskens et al., 2016). Figure 30 and 31 show this is not so. The standard deviation of GEM is about 2 km/s (Table 1b) and 190 meteors over 37.62 km/s (the lowest DRG) could exist in the total of CAMS' 4960 Geminids. CAMS wrote that the mean velocity of DRG is 7σ

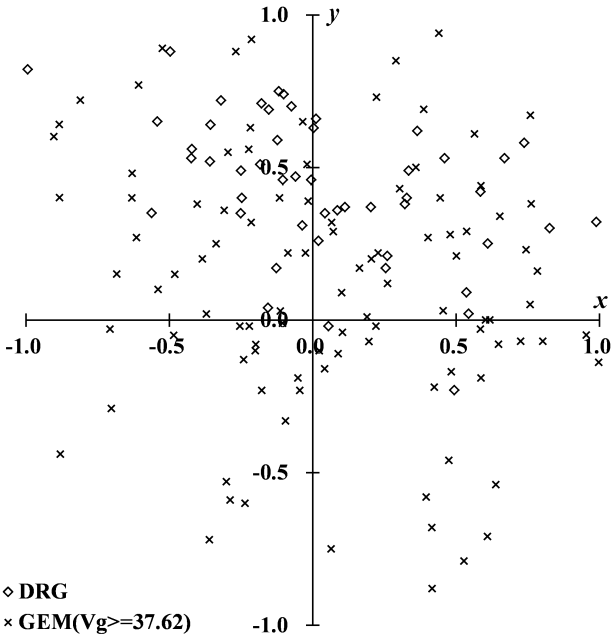

Figure 31 – Radiant distributions of DRG and GEM meteors faster than $V_g > 37.62$ km/s centered at $(\lambda - \lambda_\odot, \beta) = (208, 10)$.

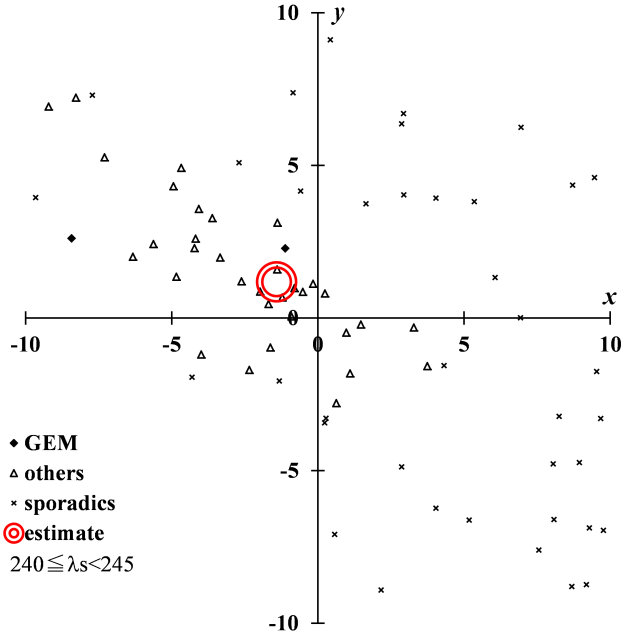

Figure 32 – Radiant distribution of early Geminids or THA based on CAMS' classification centered at $(\lambda - \lambda_\odot, \beta) = (208, 10)$.

higher than that of GEM, though σ of GEM velocities is about 2. CAMS's σ may refer to the confidence interval of the mean and not to the data distribution itself. The radiant distribution of such high velocity GEM meteors coincides with DRG's (Figure 31). Because meteors radiating from the same radiant point have different orbits if their velocity differs, the difference in their orbit could not be the basis for the distinction.

Early and late GEM activity are in confusion. Figure 32 shows the radiant distribution during $\lambda_\odot = 240 \sim 245$ of CAMS with triangles representing November θ-Aurigids (THA) in CAMS's classification. The

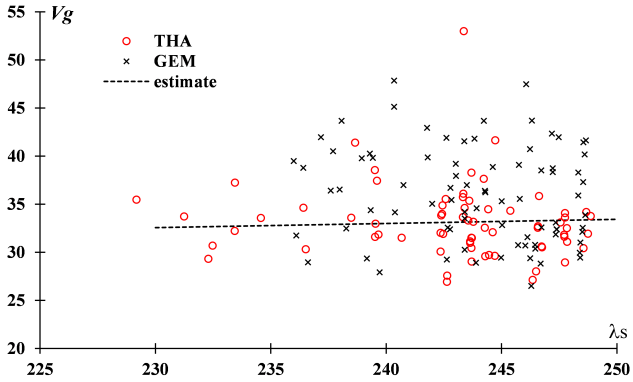

Figure 33 – Velocity distribution of early Geminids and CAMS' THA. Geminids from SonotaCo net and THA from CAMS with extended estimation by the former (dashed line).

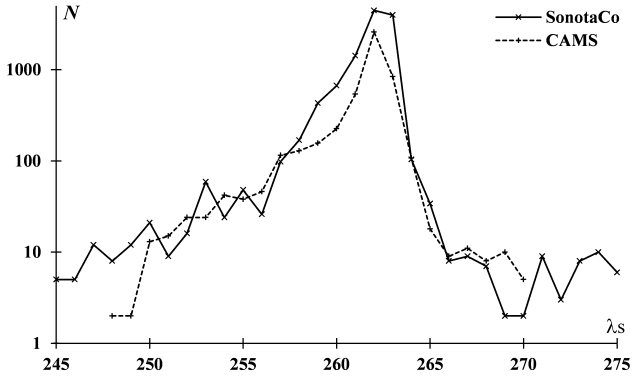

Figure 34 – Logarithmic profile of Geminid activity.

double circle in this figure means the estimation of the Geminid radiant extended from $\lambda_\odot = 255 \sim 265$ SonotaCo net observations; SonotaCo net classifies such activity as GEM naturally. We can find an interesting result from the velocity distribution (Figure 33); the dashed line indicates the extension of a linear regression of the SonotaCo net velocity between $\lambda_\odot = 255 \sim 265$. CAMS' THAs are on the dashed line, though SonotaCo's GEMs seem to be above the line. THA has been discovered by CMOR2 (Brown et al., 2010) and it is reported the maximum is $\lambda_\odot = 238$, but the number of CAMS' THA seems to increase gradually after this $\lambda_\odot$. It is necessary to study more carefully whether the activity around $\lambda_\odot = 245$ is GEM or another shower.

SonotaCo net insists GEM is active after $\lambda_\odot = 270$ but CAMS classifies them as January λ-Leonids (JLL). Figure 34 shows the logarithmic number of Geminids and the Geminid activity seems to end at $\lambda_\odot = 270$ judging from the curve. Figure 35 confirms the activity after $\lambda_\odot = 270$ might be sporadics or JLL, though JLL is weak and not distinguished from background activities.

5 Discussion

We realize both data sets of video observations are similar in their performances but the results on meteor shower surveys differ substantially, as mentioned above. Here we arrange the problems as follows: external and internal factors.

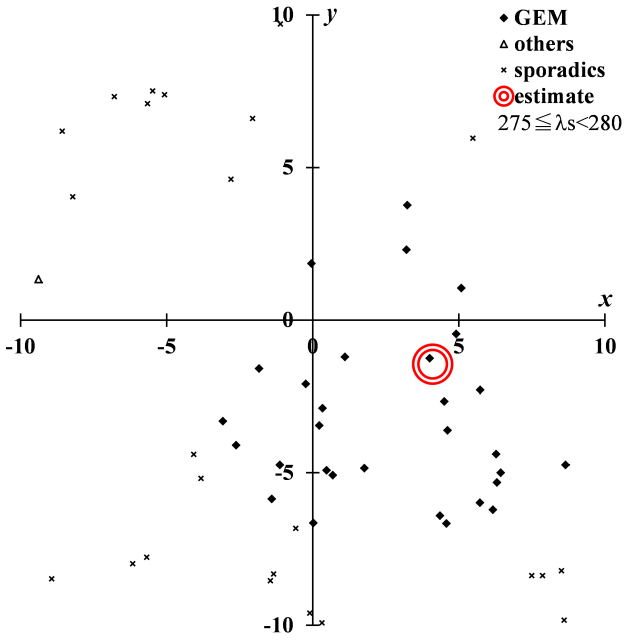

Figure 35 – Radiant distribution of late Geminids centered at $(\lambda - \lambda_\odot, \beta) = (208, 10)$ according to SonotaCo net.

5.1 External factors: Observational conditions

We find some apparent differences in the two sets of observations. We notice SonotaCo net catches more meteors at high velocity and less at low velocity compared with CAMS. This causes no strong effect on shower observations though sporadic radiant distributions are different at both ends (see radiant distributions of CAP; Figures 15a and 15b, and ORI; Figures 23a∼24b). It might be suggested SonotaCo net can find faster showers and CAMS slower ones. If we took into consideration the following factors, the two systems would show nearly equal results.

1. Weather conditions
   The rainy season from June to July (Tsuyu in Japanese) obstructs Japanese observers from continual operations. CAP and SDA are the examples; shower meteors become less and the recorded meteor numbers show the apparent maximum.

2. Suspension of operation
   We studied CAMS data of California working as a single system, though many cameras are used. The reasons of suspension at Leonid maximum are unknown but CAMS failed to catch Leonids in 2011 and 2012.

3. Missing the maximum
   We meet the true shower maximum every 4 years because Earth moves around its orbit with a fraction of 1/4 day. SonotaCo net met GEM 2012 but CAMS missed it. This is the reason why SonotaCo net recorded much more GEM than CAMS and would cause apparent differences of meteor numbers in other showers.

5.2 Internal factors: Research methods and the definition of a meteor shower

1. Radiant area and radiant drift
   The extreme case is the DAD of SonotaCo net. Though DAD is an unclear meteor shower that has dispersed radiant area without a sharp peak, SonotaCo net applies such a wide radiant definition and such a long activity period for DAD that DAD encroaches upon QUA. We noticed the originally classified shower members do not accord with the radiant estimated by the core activity in many cases. This causes the apparent long duration of the activity and the inaccurate maximum in the IAUMDC list.

2. Duration of activity
   When we use too long an activity duration for a major shower we might overlook minor showers, and vice versa when we use too short a period we might find apparent showers. CAMS tends to use shorter duration than SonotaCo net does and finds many new apparent showers, SDA and AOA for an example. On the contrary, SonotaCo net might miss XCS in Capricornids and JLL in Geminid observations.

3. Range of velocity
   Velocity distributions of PER and GEM show both CAMS and SonotaCo net have almost the same accuracy. We should be more careful before dividing a meteor shower into several parts based on the difference in velocity. CAMS might succeed in dividing XCS from CAP on the basis of the difference of $\Delta V_g = 1$ (km/s) in addition to the radiant displacement. But, on the other hand, it seems to be unreasonable in the cases of SDA and AOA.

4. How minutely we can divide a meteor shower into parts
   We discriminate meteor showers using similarity of orbits or geocentric parameters in many cases. A small change in velocity or a little displacement in radiant point corresponds naturally to a difference in orbit. We can consider that researching radiant points with their velocities is almost equivalent to studying their orbits instead. There is no absolute discrimination level in both methods and therefore the IAUMDC list can become confused by new reports.

   SonotaCo net recognizes Taurids as two showers (Northern and Southern branches according to the traditional treatment) but CAMS decomposes it into 19 individual streams. CAMS insists there are several radiant jumps and the overall distribution can be divided into parts. But as a result, CAMS's STA and NTA show very curious activity profiles as shown in Figures 27a and 27b, though inferred Taurid meteors in CAMS data express a rather natural change (Figure 27c). The radiant distribution also suggests such decomposition is inappropriate (Figures 26a and 26b). There are some gaps in CAMS observations due to adverse weather condition and the openly published CAMS observations are for two years 2011–12 only, except for imperfect years 2010 and 2013. We need ten times or more meteor data than CAMS or SonotaCo net in a year in order to confirm such jumps and subdivisions.

5.3 Future surveys

Then we need to discuss what principle is important in future surveys.

5.3.1 Major shower studies

Large quantities of data permit us to derive a more proper index, that is, not mean values over a wide range but the mode or the mean at the maximum. Researchers tend to lengthen the activity period and widen the radiant area. Mean values derived from expanded results are distorted and, therefore, the mean time of observations or the mean descending node is problematic because it indicates the maximum of activity. There are several cases in the IAUMDC list where the mean descending (or ascending) node departs from the shower maximum by several degrees.

If we want to get information of the outskirts of the activity, it would be recommended to use the shift of the radiant not in (α, δ) but in $(\lambda - \lambda_\odot, \beta)$ coordinates and of the velocity using data around 10 or 15 degrees in solar longitude from the maximum. We have studied above several showers in such a manner and get satisfactory results.

5.3.2 Occasional showers

We noticed enhanced Lyrid activity at the separated maximum in 2014 and can remember other enhanced activities of major showers as shown above. Because it is very natural that the activity intensity varies year by year, it is recommended to show the years of the observations and whether they are regular years or enhanced ones.

The Giacobinids (=October Draconids; DRA) are almost missed in both CAMS and SonotaCo net in this research. DRA is a typical periodic shower and reliable members of DRA do not appear in regular years. The Ursids (URS) are another periodic shower that raises its activity occasionally. The κ-Cygnids (KCG) shower has been well observed with a 7 year period (2007 and 2014) and the nature of its high level activity is somewhat different from regular years.

It is necessary to continue observations for longer in order to catch such enhanced or occasional activities with the same devices and system. SonotaCo net published 10 years results and CAMS will do so. We can expect new scenarios of meteor shower activities through future data releases.

5.3.3 Minor shower studies: for future survey

There are many meteor showers having working status at the IAUMDC and the number of them is becoming enormous with the development of video observations. It is necessary to set a preliminary regulation to

avoid the confusion. The author will discuss so-called 'established' showers again using SonotaCo net data and propose a regulation (Koseki, 2018). He suggests here a general idea on the basis of the above discussions.

We suggested above that the radiant area of many showers is expressed by a radius of 3 degrees in $(\lambda - \lambda_\odot, \beta)$ and more than 80% meteors are well within 3 km/s in velocity from the mean. As shown in the SDA and ORI sections, the ratio of radiant number d<3 to d>3 or to 3<d<10 is valid for excluding other (sporadic) activities.

If we select shower meteors within 5 degrees in solar longitude from the maximum, we could neglect the change of radiant point in $(\lambda - \lambda_\odot, \beta)$ coordinates and of velocity. We can limit 'shower members' to the core in this manner and get more reliable and representative data. If we intend to express the dispersion of a shower, it is necessary to get much more data and to extend the column/line of the IAUMDC list, though it would be quite complicated.

6 Conclusions

Though we find some differences in meteor shower data of SonotaCo net and CAMS, the cause is not their differences in equipment but the classification of shower members. We limited the subject to the active showers which yield enough meteors. If we extended the research to minor showers, we would meet severe difficulties of unclear shower classification as shown in the case of DAD.

It is impossible to apply the former subjective manner in searching for new meteor showers. We can easily notice the active showers such as PER and GEM but weak ones are easily overlooked or mistaken because of the concentration of radiants or in the four dimensional space of orbital elements. There might be many problematic examples in the IAUMDC list; a shower activity is recognizable but the concentration is so unclear that given results are different by each group of researchers. It is necessary to set preliminary regulation for reporting new showers; the number of meteors (orbits) and the ratio of the shower to the background. The author hopes that many meteor enthusiasts participate in the discussion and present simple and suitable regulation.

References

Brown P., Wong D. K., Weryk R. J., and Wiegert P. (2010). "A meteoroid stream survey using the Canadian Meteor Orbit Radar. II. Identification of minor showers using a 3D wavelet transform". *Icarus*, **207**, 66–81.

IAUMDC (2018). "IAU Meteor Data Center". `https://www.ta3.sk/IAUC22DB/MDC2007/` . (2018 January 13).

Jenniskens P., Nénon Q., Albers J., Gural P. S., Haberman B., Holman D., Morales R., Grigsby B. J., Samuels D., and Johannink C. (2016). "The established meteor showers as observed by CAMS". *Icarus*, **266**, 331–354.

Komaki K. (1945). "Outburst of Lyrids". *Circ. Kii Astron. Soc.*, **No.25**. (in Japanese).

Koseki M. (2012). "Three components of 'Taurids'". *WGN, the Journal of the IMO*, **40**, 129–138.

Koseki M. (2015). "What do we see as ANT, Apex and Toroidal sources? - What meteors are, where meteors came from, where meteoroids are going". *WGN, the Journal of the IMO*, **43**, 127–146.

Koseki M. (2016). "Research on the IAU meteor shower database". *WGN, the Journal of the IMO*, **44**, 151–169.

Koseki M. (2018). "IAUMDC showers viewed through SonotaCo net data". *WGN, the Journal of the IMO*. (will be submitted).

Molau S. (2010). "A new analysis of the IMO Video Meteor Database". In Kaniansky S. and Zimnikoval P., editors, *Proceedings of the International Meteor Conference, 27th IMC, Sachticka, Slovakia, 2008.* pages 76–90.

Roggemans P. (2015). "CAMS Cameras for All sky Meteor Surveillance: Manual for the CAMS BeNeLux network". `https://manualzz.com/doc/6866339/cameras-for-all-sky-meteor-surveillance-manual-for-the-cams` .

Sekanina Z. (1970). "Statistical model of meteor streams. II. Major showers". *Icarus*, **13**, 475–493.

SonotaCo (2009). "A meteor shower catalog based on video observations in 2007–2008". *WGN, Journal of the IMO*, **37**, 55–62.

SonotaCo (2017). "SonotaCo Network simultaneously observed meteor data sets". `http://sonotaco.jp/doc/SNM/` .

Southworth R. B. and Hawkins G. S. (1963). "Statistics of meteor streams". *Smithsonian Contributions to Astrophysics*, **7**, 261–285.

Whipple F. L. (1940). "Photographic meteor studies. III. The Taurid shower". *Proceeding of the American Philosophical Society*, **83**, 711–745.

Wright F. W., Jacchia L. G., and Whipple F. L. (1957). "Photographic ι-Aquarid meteors and evidence for the northern δ Aquarids". *AJ*, **62**, 225–233.

Handling Editor: David Asher

Appendix: Quick reference for IAU 3 character code.

$\lambda - \lambda_\odot$ and β are added by the author using radiant coordinate α and δ with LaSun_. LaSun means the shower maximum originally but it is inconsistent with the descending node. LaSun_ used here is derived from the descending node.

Note: Data used here are from the first line of each entry at IAUMDC, though they are not always the representative values.

IAUNo	code	shower name	$\lambda - \lambda_\odot$	β	LaSun_	V_g
00505	AIC	August iota Cetids	207.8	−7.5	145.4	37.24
00018	AND	Andromedids	162.6	20.8	231.0	17.2
00640	AOA	August omicron Aquariids	206.8	−8.7	137	38.2
00144	APS	Daytime April Piscids	338.0	0.0	30.7	28.9
00171	ARI	Daytime Arietids	328.4	7.8	77.6	35.7
00629	ATS	A2 Taurids	190.2	2.4	233.4	27.5
00635	ATU	A1 Taurids	190.5	2.4	231.2	27.4
00021	AVB	alpha Virginids	155.0	−7.1	28	17.6
00342	BPI	August Beta Piscids	208.0	6.7	140	38.3
00001	CAP	alpha Capricornids	178.0	10.7	128.9	22.2
00020	COM	Comae Berenicids	252.5	18.4	283.3	63.7
00388	CTA	chi Taurids	205.8	3.5	220.0	42.1
00334	DAD	December alpha Draconids	266.1	63.0	256.5	41.6
00631	DAT	delta Arietids	195.2	2.4	215.2	29.3
00336	DKD	December kappa Draconids	244.6	61.3	250.2	43.4
00029	DLE	delta Leonid Complex			334.7	20
00325	DLT	Daytime lambda Taurids	331.6	−8.2	181.7	36.4
00009	DRA	October Draconids	77.7	75.6	203.9	16.7
00641	DRG	December rho Geminids	207.8	10.5	261.8	39.5
00023	EGE	epsilon Geminids	254.4	3.7	209.0	68.8
00692	EQA	epsilon Aquariids	173.3	12.0	138.7	19.9
00191	ERI	eta Eridanids	260.8	−28.6	137.49	64
00031	ETA	eta Aquariids	291.2	7.6	44.44	65.9
00011	EVI	eta Virginids	186.9	3.2	280.5	29.2
00549	FAN	49 Andromedids	284.7	34.8	114.0	60.1
00286	FTA	omega Taurids	179.3	−3.3	240.2	21.7
00637	FTR	f Taurids	190.3	−4.6	225.9	27.4
00004	GEM	Geminids	207.7	10.6	261.49	34.58
00016	HYD	sigma Hydrids	228.8	−17.0	264.8	58
00644	JLL	January lambda Leonids	207.3	7.5	277.7	38.6
00667	JTP	June theta Piscids	289.3	8.9	70.2	66.6
00012	KCG	kappa Cygnids	177.0	79.6	145	24.8
00027	KSE	kappa Serpentids	206.8	35.0	15.7	45
00322	LBO	lambda Bootids	259.8	54.4	295.4	41.75
00626	LCT	lambda Cetids	193.3	−4.6	215.1	27.9
00013	LEO	Leonids	273.2	10.2	236.15	70.66
00022	LMI	Leonis Minorids	297.6	25.9	208.36	61.9
00625	LTA	lambda Taurids	187.8	−5.2	231.3	25.7
00006	LYR	April Lyrids	240.6	56.7	31.8	46.6
00019	MON	December Monocerotids	201.2	−14.8	260.2	42
00026	NDA	Northern delta Aquariids	207.1	6.4	139.0	40.5
00632	NET	November eta Taurids	191.9	2.4	227.1	28.0
00033	NIA	Northern iota Aquariids	180.9	6.8	147.7	31.2
00392	NID	November i Draconids	270.1	62.5	241.0	43
00025	NOA	Northern October delta Arietids	197.4	6.0	201.7	36.3
00152	NOC	Northern Daytime omega Cetids	321.6	15.4	47.8	33
00250	NOO	November Orionids	205.6	−7.7	247	43.7
00215	NPI	Northern delta Piscids	194.0	3.3	168.3	27.4
00017	NTA	Northern Taurids	197.0	1.3	226.2	28.3
00337	NUE	nu Eridanids	259.3	−20.7	167.9	65.9
00164	NZC	Northern June Aquilids	212.9	13.5	86.5	36.3
00153	OCE	Southern Daytime omega Cetids	330.8	−12.1	48.6	36.6
00008	ORI	Orionids	246.6	−7.4	208.6	66.2
00256	ORN	Northern chi Orionids	187.2	2.2	257.3	24.9
00257	ORS	Southern chi Orionids	179.0	−7.3	260.1	21.5
00187	PCA	psi Cassiopeiids	307.6	53.9	114.4	40.3
00642	PCE	phi Cetids	204.4	−8.1	161.1	36.5
00024	PEG	mu Pegasids	115.9	29.6	230.4	11.21
00007	PER	Perseids	282.0	38.4	139.7	59.49
00372	PPS	phi Piscids	281.7	14.5	106.0	62.9
00030	PSC	Piscid Complex			179	28
00633	PTS	p Taurids	188.8	2.4	238.6	26.7
00010	QUA	Quadrantids	277.0	63.6	283.3	41.36
00005	SDA	Southern delta Aquariids	212.0	−7.2	132.2	40.5
00003	SIA	Southern iota Aquariids	199.7	−3.5	131.7	33.8
00156	SMA	Southern Daytime May Arietids	341.9	−4.1	52.7	28.9
00028	SOA	Southern October delta Arietids	196.0	−2.6	198.5	25.6
00479	SOO	September omicron Orionids	253.6	−10.9	185.6	67.6
00208	SPE	September epsilon Perseids	248.2	20.3	171.3	64.5
00216	SPI	Southern delta Piscids	199.7	−4.4	184	26.5
00002	STA	Southern Taurids	186.5	−5.0	217.3	28
00628	STS	s Taurids	192.0	−4.7	222.1	28.2
00630	TAR	tau Arietids	193.1	2.6	220.4	28.1
00321	TCB	theta Coronae Borealids	279.2	52.4	296.5	38.66
00390	THA	November theta Aurigids	212.2	11.3	237.0	33.8
00015	URS	Ursids	218.5	72.1	270.74	33.0
00624	XAR	xi Arietids	195.1	−4.6	204.4	28.5
00323	XCB	xi Coronae Borealids	299.7	51.5	294.5	44.25
00623	XCS	xi2 Capricornids	183.7	8.8	119.7	24.5
00014	XOR	chi Orionid Complex			259	25
00243	ZCN	zeta Cancrids	254.6	−6.1	235.4	63.4
00444	ZCS	zeta Cassiopeiids	277.8	42.8	113.2	57.3
00172	ZPE	Daytime zeta Perseids	348.8	6.0	81.5	25.1

Preliminary results

Results of the IMO Video Meteor Network — October 2017

Sirko Molau[1], Stefano Crivello, Rui Goncalves, Carlos Saraiva, Enrico Stomeo, Jörg Strunk, and Javor Kac

Cameras of the IMO Video Meteor Network recorded over 66 000 meteors in more than 12 800 hours of observing time during 2017 October. The October Camelopardalids reached their short peak with a FWHM of about 20 minutes and flux density of almost 30 meteoroids per 1 000 km^2 per hour at $\lambda_\odot = 192.^\circ50$ (corresponding to 2017 October 5, 19^h20^m UT), which is around two hours earlier than in previous years. The flux density profiles and population index profiles are presented for the 2017 October Camelopardalids, October Ursae Majorids, Orionids, and Leonis Minorids.

Received 2018 July 9

1 Introduction

Following a mediocre September we enjoyed another record-breaking October in the IMO Video Network. The number of cameras was slowly growing, with the Cilbo cameras coming back into operation in late October, and the weather was also unusually pleasant. In particular southern Europe had little problem with night-time cloud, and Slovenia was also lucky this time. Germany and Poland, on the other hand, had to cope with longer breaks due to poor weather. Overall 58 of 79 cameras recorded meteors during 20 or more observing nights, Bmh2 of Maurizio Carli observed in every night.

The effective observing time amounted to over 12 800 hours and even surpassed August 2017. The output was 15% higher than in the previously best October and was the third best monthly result of the IMO Network ever. We recorded over 66 000 meteors during that time (Table 1 and Figure 1), which is an increase of over 20% to the previously best October. The average of 5.2 meteors per hour was in line with the result of the previous years, however.

October is always an interesting month thanks to the multitude of active meteor showers, some of which we will inspect more closely now.

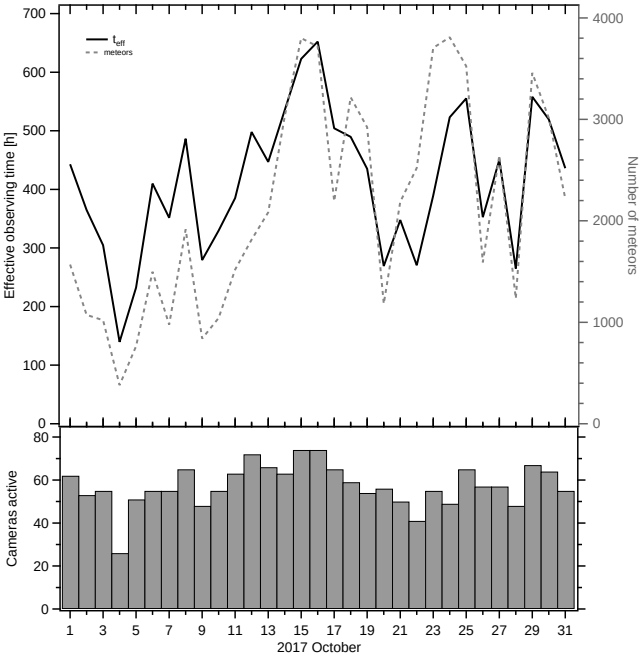

Figure 1 – Monthly summary for the effective observing time (solid black line), number of meteors (dashed gray line) and number of cameras active (bars) in 2017 October.

2 October Camelopardalids

The October Camelopardalids play a special role since their nature is still under discussion. They have a very small full width at half maximum (FWHM) and can thus be observed only every other year when the peak falls into the night time hours of the corresponding location. Some researchers state that the Camelopardalids are only occasionally active, whereas we believe in a shower that returns annually. The average profile of 2011–2016 shows a peak at $192.^\circ59$ solar longitude (Figure 2, lighter/green) with a peak flux density of about 7 meteoroids per 1 000 km^2 per hour and a FWHM of less than $0.^\circ2$ solar longitude (< 5 hours). The peak was expected to be well seen from Europe on 2017 October 5, near 21^h30^m UT. The Camelopardalids did indeed reach their peak during the evening hours, but somewhat earlier and much stronger than anticipated (Figure 2, darker/red). At 19^h20^m UT ($192.^\circ50$ solar longitude) we could briefly measure a flux density of almost 30 meteoroids per 1 000 km^2 per hour. The FWHM was only $0.^\circ015$ solar longitude, corresponding to about 20 minutes.

Due to the short duration, the activity profile relies on a small data set – in this case about 60 shower meteors in total that were recorded by the IMO Network cameras. To make sure these were not false detections by a single camera or similar artifacts, we inspected the relevant data set manually. Indeed, there were about a dozen cameras in Germany, Italy, Hungary and Portugal with clear skies during the first two evening hours that clearly recorded more October Camelopardalids than sporadic or other shower meteors. Thus, the ac-

[1]Abenstalstr. 13b, 84072 Seysdorf, Germany.
Email: sirko@molau.de

IMO bibcode WGN-464-molau-vidoct
NASA-ADS bibcode 2018JIMO...46..136M

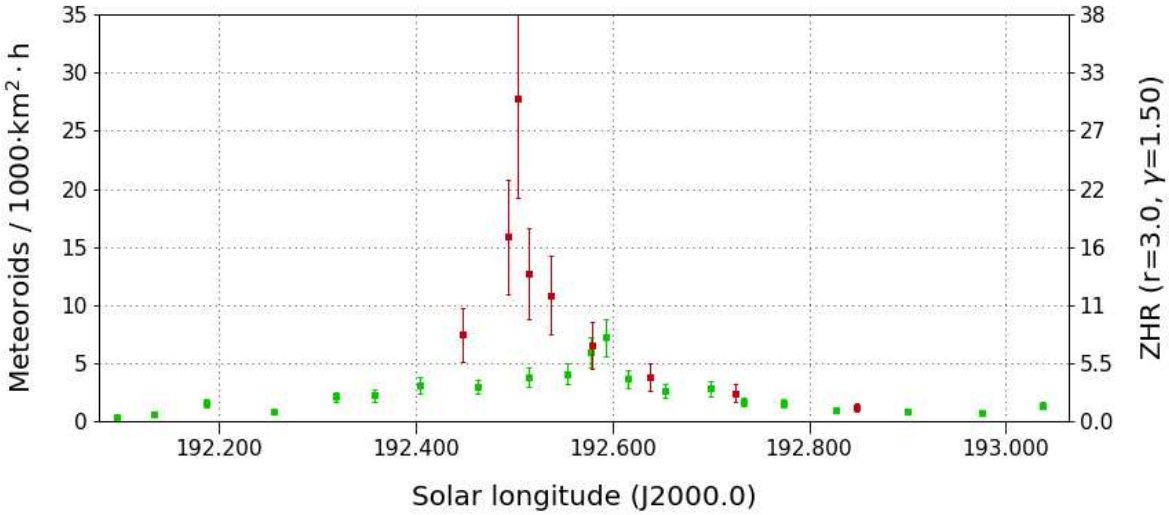

Figure 2 – Comparison of the flux density profile of the October Camelopardalids 2011–2016 (lighter/green) and 2017 (darker/red), derived from video data of the IMO Network.

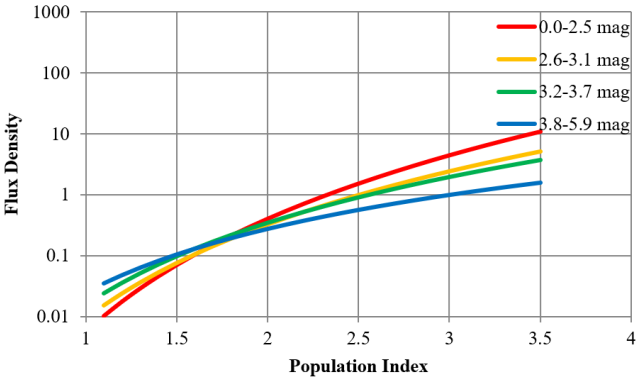

Figure 3 – Population index of the October Camelopardalids. The individual flux density profiles intersect exactly at one point with $r = 1.75$.

tivity peak was real and the equivalent ZHR (eZHR) reached almost 30 for a short period of time.

To determine the population index of the October Camelopardalids we had to combine the observations from 2011 to 2017. The data set of about 300 shower meteors yielded in total a population index of $r = 1.75$ (Figure 3). During the same time frame, the average population index for sporadic meteors was higher than 2.5, i.e. the Camelopardalids contain a large fraction of bright meteors.

3 October Ursae Majorids

At the middle of October, we may observe the October Ursae Majorids. In the long-term activity profile, this shower peaks at $202\overset{\circ}{.}2$ solar longitude (2017 October 15, 15^{h} UT) with a flux density of slightly more than four meteoroids per 1 000 km^2 per hour. The peak could not be observed this year, but we recorded about the same flux density of three in the nights before and after the peak (Figure 4). Since the peak of the October Ursae Majorids occurred just before new moon and we have seen systematically lower flux densities at this lunar phase, the lower activity level of 2017 seems not to be significant.

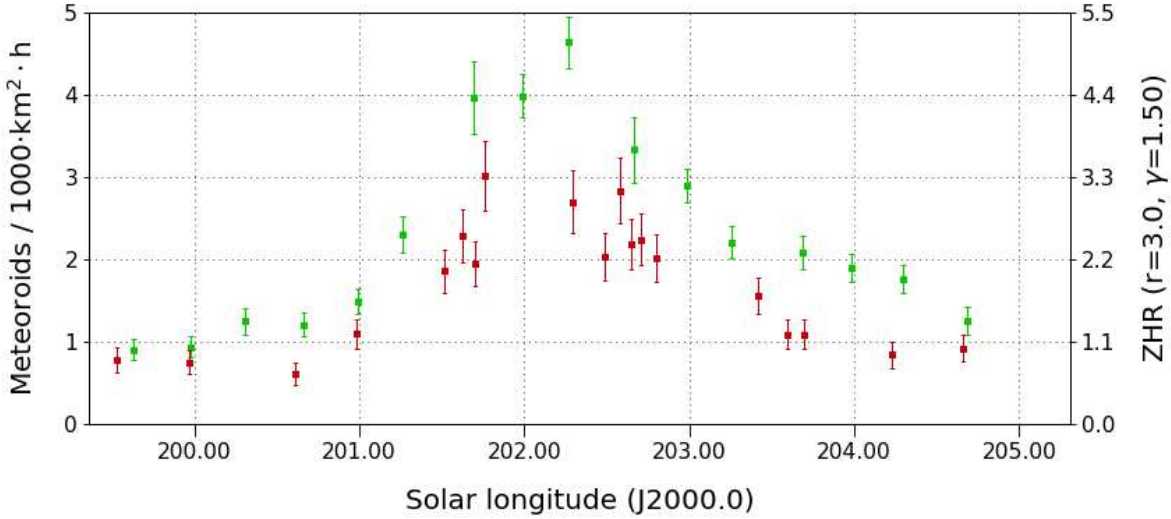

Figure 4 – Flux density profile of the October Ursae Majorids 2011–2016 (lighter/green) and 2017 (darker/red), derived from video data of the IMO Network.

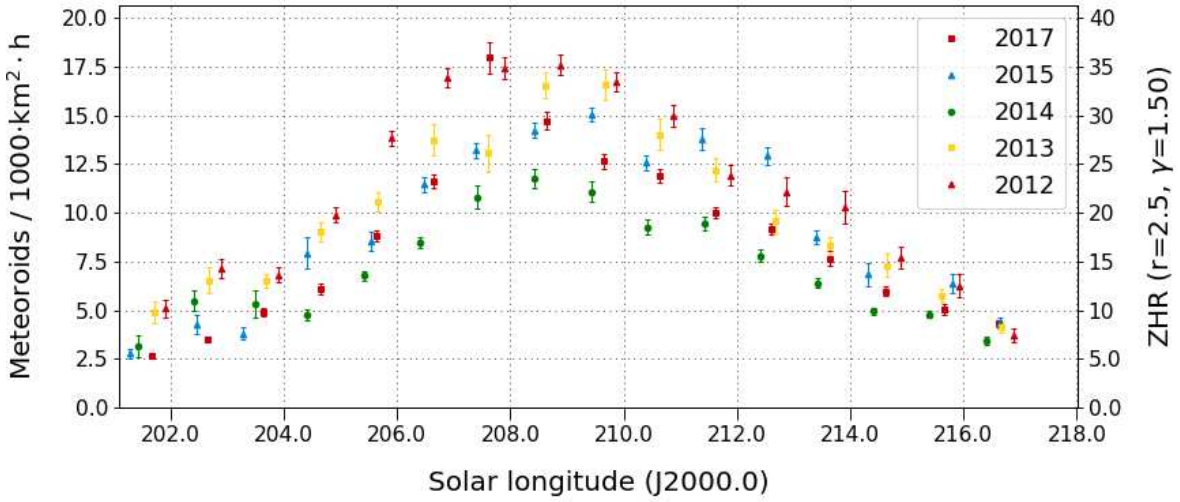

Figure 5 – Comparison of the Orionid flux density in individual years, derived from video data of the IMO Network.

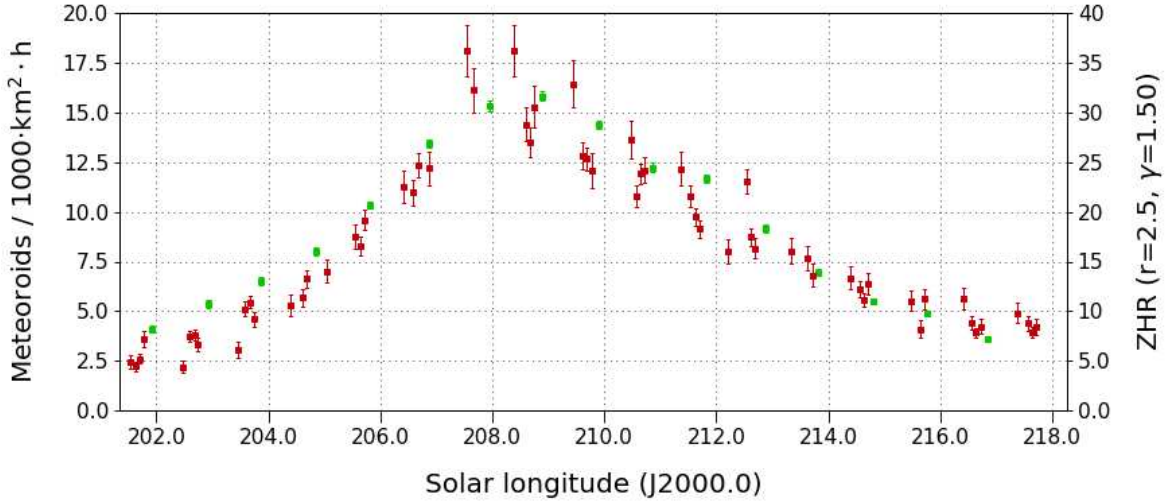

Figure 6 – Flux density profile of the Orionids 2012–2016 (lighter/green) and 2017 (darker/red), derived from video data of the IMO Network.

4 Orionids

The same is true for the Orionids which peaked a few days later. They were undisturbed by the moon and presented lower flux densities as well. Figure 5 shows that the activity profiles look nearly identical each year, but the absolute level of activity differs. In years with favorable lunar conditions (2014, 2017) the activity is virtually lower, and in years with full or waning moon as in 2013 virtually higher.

Orionid activity profiles can only be merged if the bin size is at least one degree in solar longitude such that each data point covers observations from every year. Figure 6 compares the activity profile of 2017 with the average profile of the years 2012 to 2016. In the ascending and the first half of the descending branch the flux density is somewhat lower than average and at the peak slightly higher.

5 Leonis Minorids

The Leonis Minorids reach their peak in the long-term average at the same time as the Orionids (208° solar longitude) and thus three days earlier than listed in the IMO Working List (Rendtel, 2016). This year they showed a peak at both 208° and 210° solar longitude (Figure 7), whereby there is some scatter.

With respect to the population index, the October Ursae Majorids, Orionids and Leonis Minorids are quite similar (Figure 8). Even though data from all years are averaged, the r-profiles show significant scatter that occurs synchronously at shower and sporadic meteors. These are systematic deviations with a still unknown root cause. The population index of the October Ursae Majorids and Leonis Minorids is $r = 1.95$, and of the Orionids $r = 2.15$. The mean sporadic population index is $r = 2.45$ in all three cases.

References

Rendtel J. (2016). "2017 Meteor Shower Calendar". International Meteor Organization. IMO INFO(2-16).

Handling Editor: Javor Kac

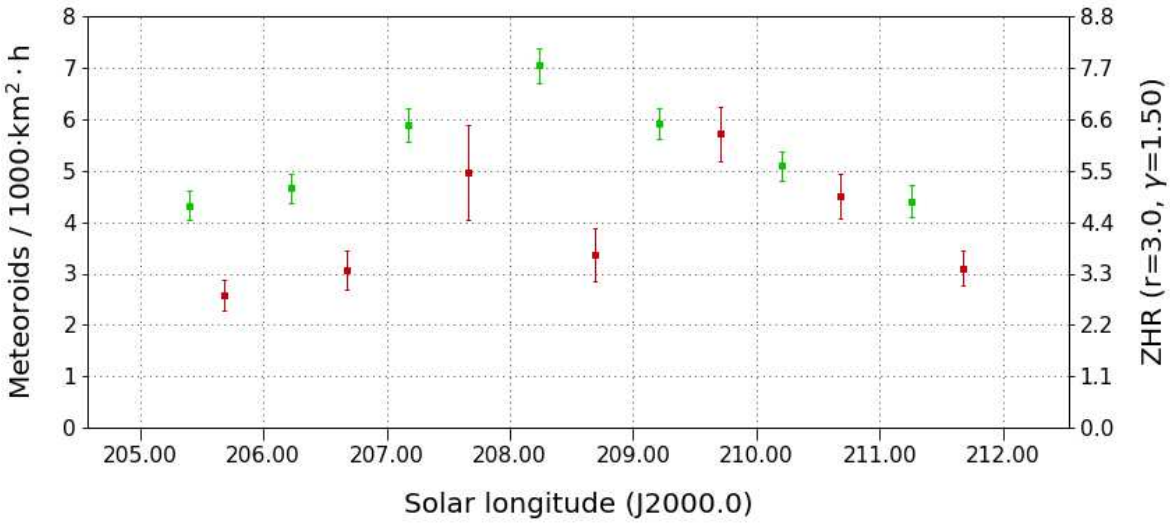

Figure 7 – Flux density profile of the Leonis Minorids 2011–2016 (lighter/green) and 2017 (darker/red), derived from video data of the IMO Network.

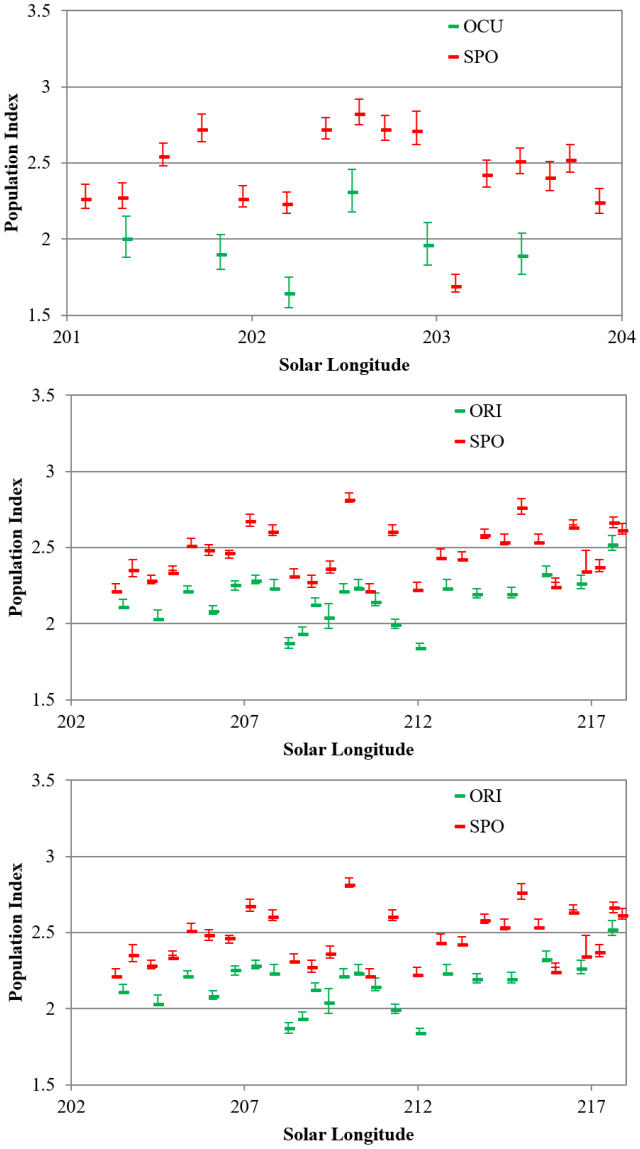

Figure 8 – Mean population index profile of the October Ursae Majorids (top), Orionids (middle) and Leonis Minorids (bottom), derived from data of 2011–2017. The *r*-value of the meteor shower is depicted in lighter/green, that of the sporadic meteors is in darker/red.

Code	Name	Location	Camera	FOV [°²]	Stellar LM [mag]	Eff.CA [km²]	Nights	Time [h]	Meteors
ARLRA	Arlt	Ludwigsfelde/DE	Ludwig2 (0.8/8)	1475	6.2	3779	25	133.7	930
BERER	Berkó	Ludányhalászi/HU	Hulud1 (0.8/3.8)	5542	4.8	3847	16	140.0	759
BOMMA	Bombardini	Faenza/IT	Mario (1.2/4.0)	5794	3.3	739	28	243.1	1590
BREMA	Breukers	Hengelo/NL	Mbb3 (0.75/6)	2399	4.2	699	21	90.4	315
BRIBE	Klemt	Herne/DE	Hermine (0.8/6)	2374	4.2	678	20	117.2	478
		Bergisch Gladbach/DE	Klemoi (0.8/6)	2286	4.6	1080	22	117.4	497
CARMA	Carli	Monte Baldo/IT	Bmh2 (1.5/4.5)*	4243	3.0	371	31	297.0	2871
CASFL	Castellani	Monte Baldo/IT	Bmh1 (0.8/6)	2350	5.0	1611	28	281.4	1304
CINFR	Cineglosso	Faenza/IT	Jenni (1.2/4)	5886	3.9	1222	27	152.8	1772
CRIST	Crivello	Valbrevenna/IT	Arci (0.8/3.8)	5566	4.6	2575	29	236.2	1428
			Bilbo (0.8/3.8)	5458	4.2	1772	29	238.2	1882
			C3P8 (0.8/3.8)	5455	4.2	1586	28	221.0	1164
			Stg38 (0.8/3.8)	5614	4.4	2007	30	249.0	2512
ELTMA	Eltri	Venezia/IT	Met38 (0.8/3.8)	5631	4.3	2151	19	141.1	647
FORKE	Förster	Carlsfeld/DE	Akm3 (0.75/6)	2375	5.1	2154	12	75.5	645
GONRU	Goncalves	Foz do Arelho/PT	Farelho1 (0.75/4.5)	2286	3.0	208	20	156.6	179
		Tomar/PT	Templar1 (0.8/6)	2179	5.3	1842	28	259.7	1596
			Templar2 (0.8/6)	2080	5.0	1508	27	264.0	1311
			Templar3 (0.8/8)	1438	4.3	571	26	240.6	551
			Templar4 (0.8/3.8)	4475	3.0	442	26	249.2	1259
			Templar5 (0.75/6)	2312	5.0	2259	26	225.2	1176
GOVMI	Govedič	Središče ob Dravi/SI	Orion2 (0.8/8)	1447	5.5	1841	29	218.8	958
			Orion4 (0.95/5)	2662	4.3	1043	14	91.6	196
HERCA	Hergenrother	Tucson/US	Salsa3 (0.8/3.8)	2336	4.1	544	30	286.0	1277
HINWO	Hinz	Schwarzenberg/DE	Hinwo1 (0.75/6)	2291	5.1	1819	16	104.0	587
IGAAN	Igaz	Hódmezővásárhely/HU	Huhod (0.8/3.8)	5502	3.4	764	15	69.0	156
			Hupol (1.2/4)	3790	3.3	475	21	159.1	166
JONKA	Jonas	Budapest/HU	Husor (0.95/4)	2286	3.9	445	26	180.8	501
			Husor2 (0.95/3.5)	2465	3.9	715	26	216.3	495
KACJA	Kac	Ljubljana/SI	Orion1 (0.8/8)	1399	3.8	268	25	216.0	1289
		Kamnik/SI	Cvetka (0.8/3.8)*	4914	4.3	1842	26	193.7	1336
			Rezika (0.8/6)	2270	4.4	840	25	209.7	2280
			Stefka (0.8/3.8)	5471	2.8	379	22	178.1	931
		Kostanjevec/SI	Metka (0.8/12)*	715	6.4	640	27	253.0	1280
KOSDE	Koschny	Izana Obs./ES	Icc7 (0.85/25)*	714	5.9	1464	7	57.9	367
			Lic1 (2.8/50)*	2255	6.2	5670	6	48.2	470
		La Palma/ES	Icc9 (0.85/25)*	683	6.7	2951	4	29.5	638
LOPAL	Lopes	Lisbon/PT	Naso1 (0.75/6)	2377	3.8	506	16	124.4	225
MACMA	Maciejewski	Chełm/PL	Pav35 (0.8/3.8)	5495	4.0	1584	13	53.0	235
			Pav36 (0.8/3.8)*	5668	4.0	1573	14	90.3	416
			Pav43 (0.75/4.5)*	3132	3.1	319	14	5.6	28
			Pav60 (0.75/4.5)	2250	3.1	281	14	92.9	435

Table 1 – Observers contributing to 2017 October data of the IMO Video Meteor Network. Eff.CA designates the effective collection area; the overall number of nights is the number of nights with at least one camera operating, the overall observing time and number of meteors are sums over all cameras.

Table 1 – Observers contributing to 2017 October data of the IMO Video Meteor Network – continued from previous page.

Code	Name	Location	Camera	FOV [°²]	Stellar LM [mag]	Eff.CA [km²]	Nights	Time [h]	Meteors
MARRU	Marques	Lisbon/PT	Cab1 (0.75/6)	2362	4.8	1517	29	260.8	1441
			Ran1 (1.4/4.5)	4405	4.0	1241	26	227.4	1021
MASMI	Maslov	Novosibirsk/RU	Nowatec (0.8/3.8)	5574	3.6	773	17	113.3	553
MOLSI	Molau	Seysdorf/DE	Avis2 (1.4/50)*	1230	6.9	6152	26	183.8	1814
			Escimo2 (0.85/25)	155	8.1	3415	13	107.3	283
			Mincam1 (0.8/8)	1477	4.9	1084	16	113.2	604
		Ketzür/DE	Remo1 (0.8/8)	1467	6.5	5491	22	123.4	883
			Remo2 (0.8/8)	1478	6.4	4778	23	141.9	1113
			Remo3 (0.8/8)	1420	5.6	1967	24	158.8	942
			Remo4 (0.8/8)	1478	6.5	5358	26	158.5	1301
MOSFA	Moschini	Rovereto/IT	Rover (1.4/4.5)	3896	4.2	1292	27	228.5	685
OCHPA	Ochner	Albiano/IT	Albiano (1.2/4.5)	2944	3.5	358	19	138.4	606
OTTMI	Otte	Pearl City/US	Orie1 (1.4/5.7)	3837	3.8	460	20	132.1	305
PERZS	Perkó	Becsehely/HU	Hubec (0.8/3.8)*	5498	2.9	460	28	237.8	1641
ROTEC	Rothenberg	Berlin/DE	Armefa (0.8/6)	2366	4.5	911	21	134.5	437
SARAN	Saraiva	Carnaxide/PT	Ro1 (0.75/6)	2362	3.7	381	29	198.7	526
			Ro2 (0.75/6)	2381	3.8	459	28	220.4	817
			Ro3 (0.8/12)	710	5.2	619	28	239.6	1022
			Ro4 (1.0/8)	1582	4.2	549	28	175.3	360
			Sofia (0.8/12)	738	5.3	907	29	209.2	583
SCALE	Scarpa	Alberoni/IT	Leo (1.2/4.5)*	4152	4.5	2052	24	144.6	230
SCHHA	Schremmer	Niederkrüchten/DE	Doraemon (0.8/3.8)	4900	3.0	409	23	119.9	463
SLAST	Slavec	Ljubljana/SI	Kayak1 (1.8/28)	563	6.2	1294	26	151.6	1054
			Kayak2 (0.8/12)	741	5.5	920	25	210.9	288
STOEN	Stomeo	Scorze/IT	Min38 (0.8/3.8)	5566	4.8	3270	26	155.1	1242
			Noa38 (0.8/3.8)	5609	4.2	1911	28	170.1	1018
			Sco38 (0.8/3.8)	5598	4.8	3306	27	173.7	1148
STRJO	Strunk	Herford/DE	Mincam2 (0.8/6)	2354	5.4	2751	24	117.2	869
			Mincam3 (0.8/6)	2338	5.5	3590	20	98.1	436
			Mincam4 (0.8/6)	2306	5.0	1412	22	109.9	247
			Mincam5 (0.8/6)	2349	5.0	1896	21	105.6	511
			Mincam6 (0.8/6)	2395	5.1	2178	18	95.3	429
TEPIS	Tepliczky	Agostyán/HU	Huago (0.75/4.5)	2427	4.4	1036	19	149.3	516
			Humob (0.8/6)	2388	4.8	1607	24	177.3	762
WEGWA	Wegrzyk	Nieznaszyn/PL	Pav78 (0.8/6)	2286	4.0	778	23	90.0	375
YRJIL	Yrjölä	Kuusankoski/FI	Finexcam (0.8/6)	2337	5.5	3574	15	68.9	280
ZAKJU	Zakrajšek	Petkovec/SI	Tacka (0.8/12)	714	5.3	783	27	200.2	534
* active field of view smaller than video frame						Overall	31	12 847.8	66 471

Results of the IMO Video Meteor Network — November 2017

Sirko Molau[1], *Stefano Crivello, Rui Goncalves, Carlos Saraiva, Enrico Stomeo, Jörg Strunk, and Javor Kac*

The IMO Video Meteor Network cameras recorded over 46 000 meteors in more than 10 000 hours of observing time during 2017 November. The flux density profiles and population index profiles are presented for the 2017 Northern and Southern Taurids, and Leonids.

Received 2018 August 26

1 Introduction

As in the preceding month, we managed to collect more than 10 000 hours of effective observing time in November 2017. We clearly missed the record result of November 2015 (12 000 hours), but it was still the second-best result for this month. Eighty cameras recorded a total of over 42 000 meteors (Table 1 and Figure 1), which was also the second-best ever November outcome.

About half of the cameras were active during twenty and more observing nights, but no camera got more than 28 nights.

2 Taurids

November marks the nominal end of the Taurids – thereafter the activity is assigned to the Anthelion source once again. Figure 2 shows the two-months flux density profile of the Taurids. As usual the Southern Taurids (darker/red) dominate until the last ten days of October. They are then in decline, with the Northern Taurids (lighter/green) taking over and becoming the dominating branch until the end of the activity interval.

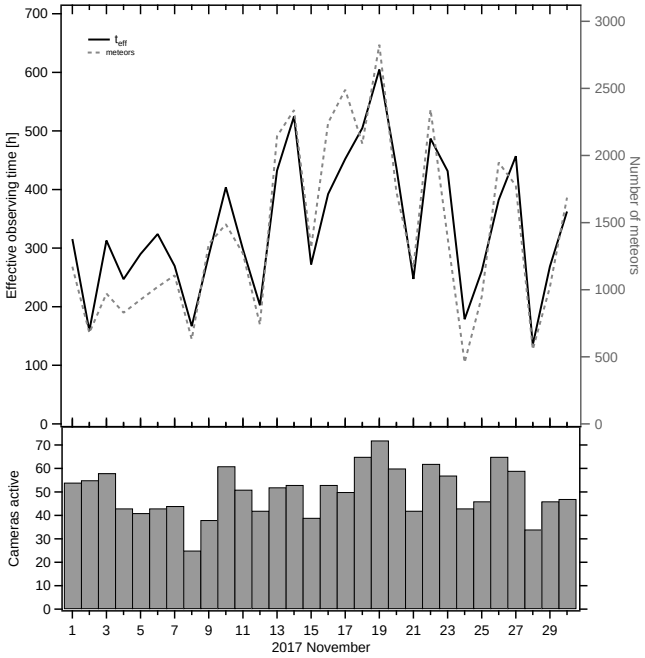

Figure 1 – Monthly summary for the effective observing time (solid black line), number of meteors (dashed gray line) and number of cameras active (bars) in 2017 November.

[1]Abenstalstr. 13b, 84072 Seysdorf, Germany.
Email: sirko@molau.de

IMO bibcode WGN-464-molau-vidnov
NASA-ADS bibcode 2018JIMO...46..142M

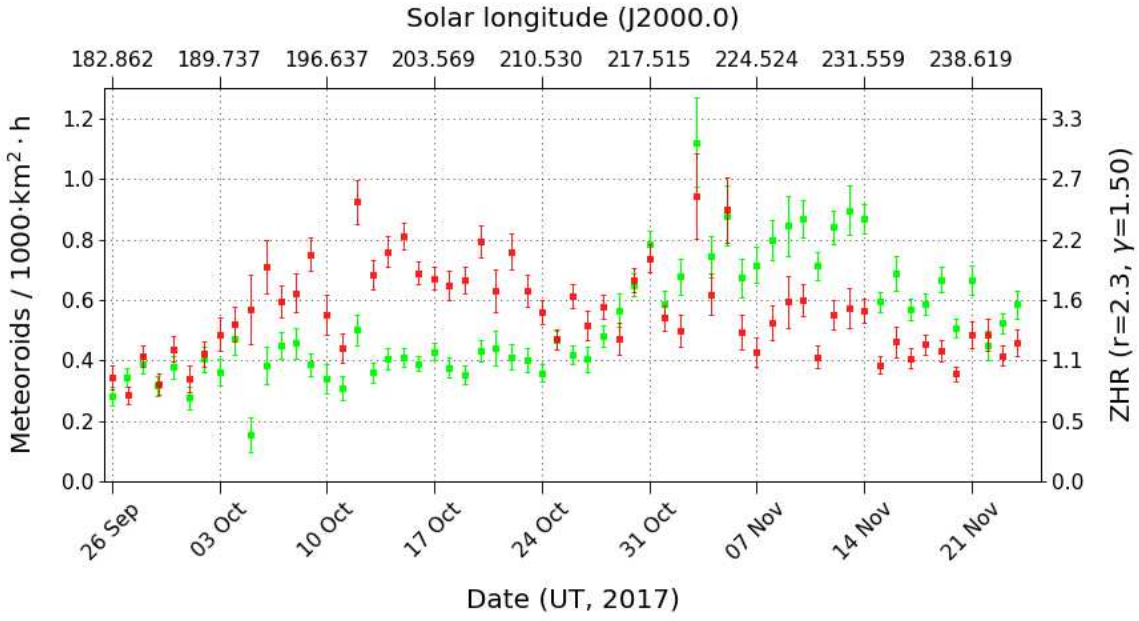

Figure 2 – Comparison of the flux density profile of the Northern (lighter/green) and Southern (darker/red) Taurids in 2017, derived from video data of the IMO Network.

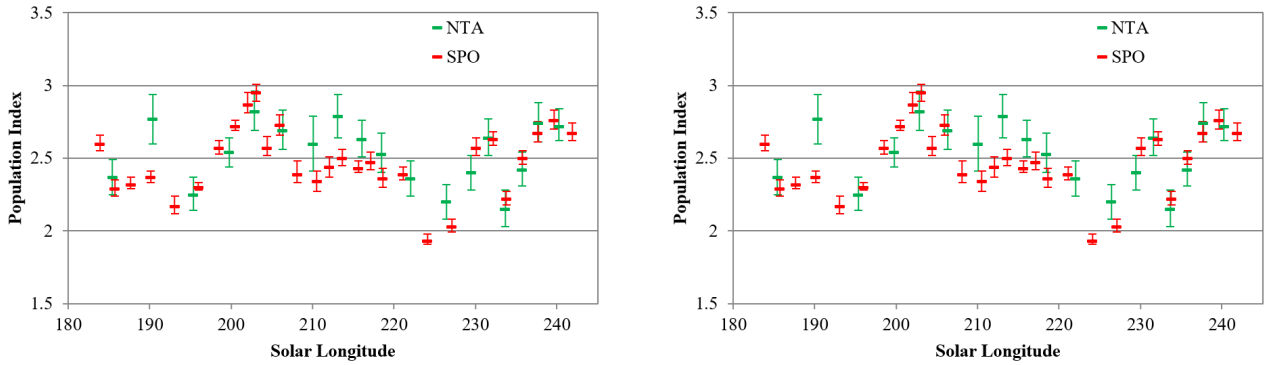

Figure 3 – Comparison of the population index profile of the Northern (lighter/green, left) and Southern (lighter/green, right) Taurids with the sporadic meteors (darker/red) in 2017.

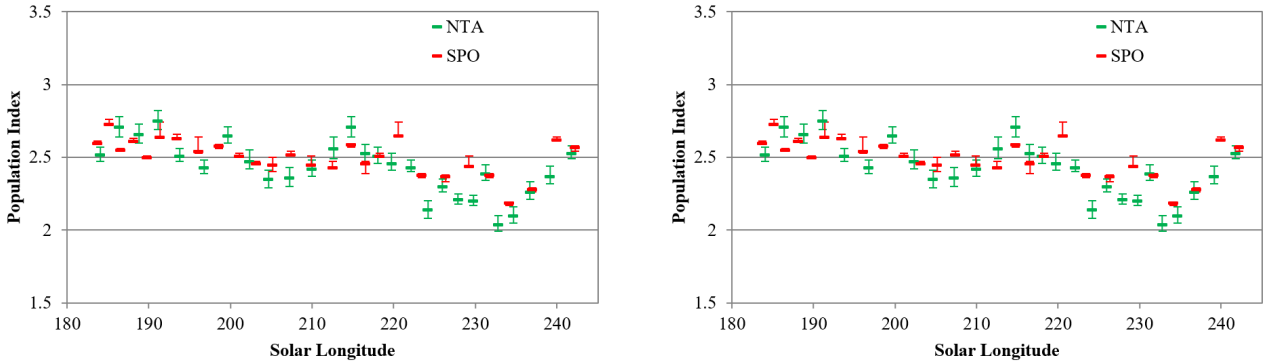

Figure 4 – Comparison of the population index profile of the Northern (lighter/green, left) and Southern (lighter/green, right) Taurids with the sporadic meteors (darker/red) in the years 2011–2017.

A look at the population index (Figure 3) shows a specialty of the Taurids. Whereas the population index of all other analyzed showers is smaller than the sporadic r-value, the population index of the Northern Taurids (left, lighter/green) is almost identical to the sporadic value (left, darker/red). In both cases, the average is $r = 2.5$. The scatter results from the different lunar phases. With $r = 2.8$ the Southern Taurids have even a larger population index than the sporadic meteors. That contradicts the IMO meteor shower working list (Rendtel, 2016), in which both branches are listed with a population index of $r = 2.3$.

Even when the average population index of the years 2011–2017 (without 2015, when the Taurid swarm occurred) is calculated, the discrepancy remains (Figure 4). Here, also, the r-value of the Northern Taurids is nearly identical with that for sporadic meteors, whereas for the Southern Taurids it is larger, by up to 0.5, and does not reach the sporadic population index value until the end of their activity period.

3 Leonids

The activity profile of the Leonids matches to the mean profile of the previous years (Figure 5). Leonid activity starts at 233° solar longitude (November 15), peaks between 235° and 238° solar longitude (November 17–20) and vanishes at 241° solar longitude (November 23) into the sporadic background. Since the Leonid peak of 2017 coincided with new moon, we observed slightly smaller rates than in the long-term average.

The Leonids are renowned for their low population index – the values measured in 2017 are still extraordinary. There average value of $r = 1.5$ smaller by 1.0 than the sporadic population index (Figure 6, left). In addition, in the long-term average of 2011–2017 the population index of the Leonids is quite low, but the 0.7 difference from the sporadic meteors is somewhat smaller (Figure 6, right).

Hence, whereas cameras with a good limiting magnitude (and with typically a small field of view) are preferred for the Taurids, you gain best results with a large field of view in case of the Leonids, given their large percentage of bright meteors.

References

Rendtel J. (2016). "2017 Meteor Shower Calendar". International Meteor Organization. IMO INFO(2-16).

Handling Editor: Javor Kac

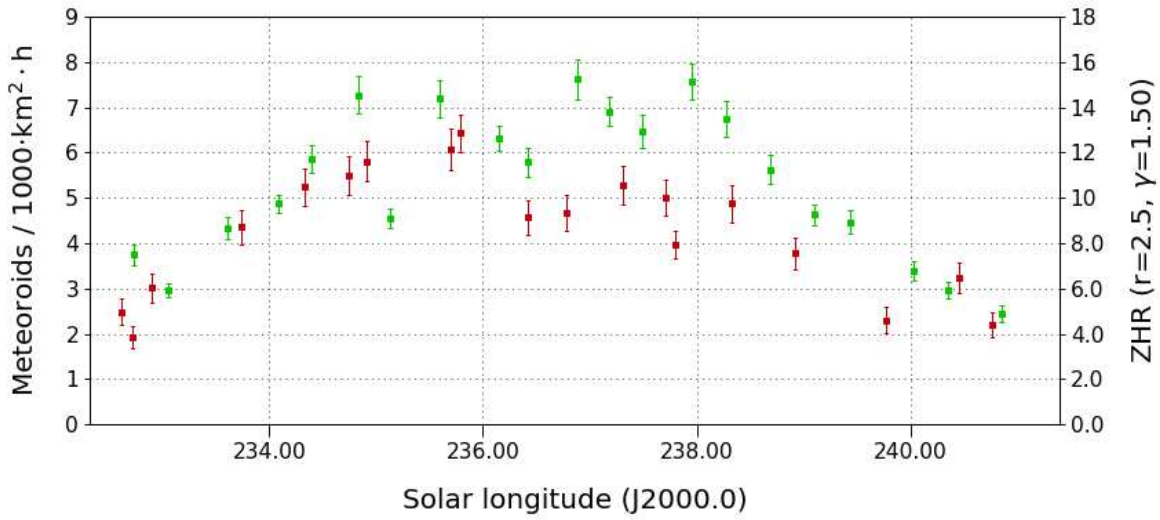

Figure 5 – Flux density profile of the Leonids 2011–2016 (lighter/green) and 2017 (darker/red), derived from video data of the IMO Network.

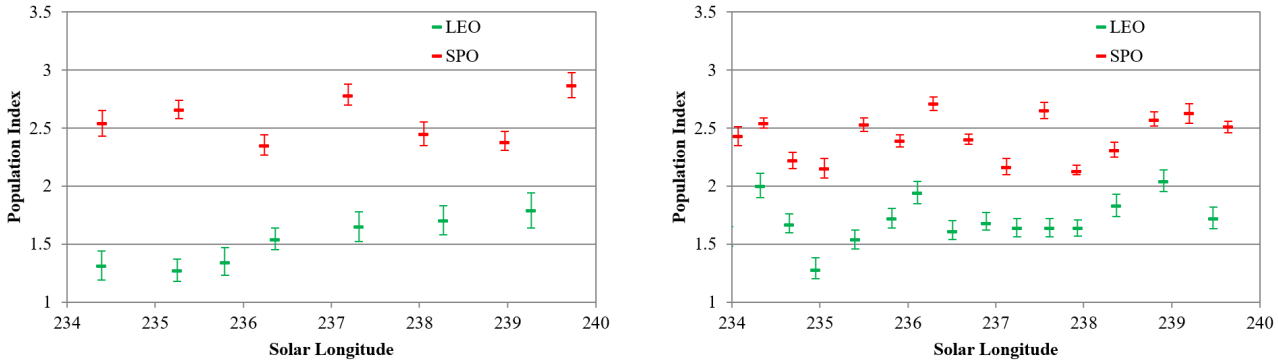

Figure 6 – Comparison of the population index profile of the Leonids (lighter/green) and sporadic meteors (darker/red) in 2017 (left) and in the years 2011–2017 (right).

Code	Name	Location	Camera	FOV [°²]	Stellar LM [mag]	Eff.CA [km²]	Nights	Time [h]	Meteors
ARLRA	Arlt	Ludwigsfelde/DE	Ludwig2 (0.8/8)	1475	6.2	3779	21	107.2	644
BERER	Berkó	Ludányhalászi/HU	Hulud1 (0.8/3.8)	5542	4.8	3847	8	83.2	536
BOMMA	Bombardini	Faenza/IT	Mario (1.2/4.0)	5794	3.3	739	24	153.4	827
BREMA	Breukers	Hengelo/NL	Mbb3 (0.75/6)	2399	4.2	699	18	70.0	180
BRIBE	Klemt	Herne/DE	Hermine (0.8/6)	2374	4.2	678	21	105.6	329
		Bergisch Gladbach/DE	Klemoi (0.8/6)	2286	4.6	1080	15	67.1	207
CARMA	Carli	Monte Baldo/IT	Bmh2 (1.5/4.5)*	4243	3.0	371	20	207.3	1572
CASFL	Castellani	Monte Baldo/IT	Bmh1 (0.8/6)	2350	5.0	1611	21	203.5	698
CINFR	Cineglosso	Faenza/IT	Jenni (1.2/4)	5886	3.9	1222	24	87.1	877
CRIST	Crivello	Valbrevenna/IT	Arci (0.8/3.8)	5566	4.6	2575	22	131.1	650
			Bilbo (0.8/3.8)	5458	4.2	1772	25	162.5	821
			C3P8 (0.8/3.8)	5455	4.2	1586	24	145.4	558
			Stg38 (0.8/3.8)	5614	4.4	2007	25	181.9	1242
ELTMA	Eltri	Venezia/IT	Met38 (0.8/3.8)	5631	4.3	2151	15	127.2	597
FORKE	Förster	Carlsfeld/DE	Akm3 (0.75/6)	2375	5.1	2154	9	41.0	187
GONRU	Goncalves	Foz do Arelho/PT	Farelho1 (0.75/4.5)	2286	3.0	208	25	191.2	179
		Tomar/PT	Templar1 (0.8/6)	2179	5.3	1842	24	250.5	1297
			Templar2 (0.8/6)	2080	5.0	1508	26	248.9	1072
			Templar3 (0.8/8)	1438	4.3	571	27	252.9	572
			Templar4 (0.8/3.8)	4475	3.0	442	26	246.2	1136
			Templar5 (0.75/6)	2312	5.0	2259	27	239.3	1058
GOVMI	Govedič	Središče ob Dravi/SI	Orion2 (0.8/8)	1447	5.5	1841	16	89.2	280
			Orion4 (0.95/5)	2662	4.3	1043	10	49.2	102
HERCA	Hergenrother	Tucson/US	Salsa3 (0.8/3.8)	2336	4.1	544	28	258.2	837
HINWO	Hinz	Schwarzenberg/DE	Hinwo1 (0.75/6)	2291	5.1	1819	18	74.2	236
IGAAN	Igaz	Hódmezővásárhely/HU	Huhod (0.8/3.8)	5502	3.4	764	16	99.1	160
			Hupol (1.2/4)	3790	3.3	475	12	52.7	53
JONKA	Jonas	Budapest/HU	Husor (0.95/4)	2286	3.9	445	15	71.2	178
			Husor2 (0.95/3.5)	2465	3.9	715	15	93.0	184
KACJA	Kac	Ljubljana/SI	Orion1 (0.8/8)	1399	3.8	268	9	44.0	113
		Kamnik/SI	Cvetka (0.8/3.8)*	4914	4.3	1842	11	61.1	229
			Rezika (0.8/6)	2270	4.4	840	12	87.3	692
			Stefka (0.8/3.8)	5471	2.8	379	10	71.5	222
		Kostanjevec/SI	Metka (0.8/12)*	715	6.4	640	12	112.6	426
KOSDE	Koschny	Izana Obs./ES	Icc7 (0.85/25)*	714	5.9	1464	23	163.5	709
			Lic1 (2.8/50)*	2255	6.2	5670	25	192.3	1005
		La Palma/ES	Icc9 (0.85/25)*	683	6.7	2951	21	143.8	1533
			Lic2 (3.2/50)*	2199	6.5	7512	5	30.6	219
MACMA	Maciejewski	Chełm/PL	Pav35 (0.8/3.8)	5495	4.0	1584	16	47.2	168
			Pav36 (0.8/3.8)*	5668	4.0	1573	16	93.1	293
			Pav43 (0.75/4.5)*	3132	3.1	319	15	43.6	172
			Pav60 (0.75/4.5)	2250	3.1	281	17	97.8	361

Table 1 – Observers contributing to 2017 November data of the IMO Video Meteor Network. Eff.CA designates the effective collection area; the overall number of nights is the number of nights with at least one camera operating, the overall observing time and number of meteors are sums over all cameras.

Table 1 – Observers contributing to 2017 November data of the IMO Video Meteor Network – continued from previous page.

Code	Name	Location	Camera	FOV [°²]	Stellar LM [mag]	Eff.CA [km²]	Nights	Time [h]	Meteors
MARRU	Marques	Lisbon/PT	CAB1 (0.75/6)	2362	4.8	1517	28	260.3	1248
			RAN1 (1.4/4.5)	4405	4.0	1241	25	214.4	1006
MASMI	Maslov	Novosibirsk/RU	NOWATEC (0.8/3.8)	5574	3.6	773	2	6.1	35
MOLSI	Molau	Seysdorf/DE	AVIS2 (1.4/50)*	1230	6.9	6152	17	96.4	785
			ESCIMO2 (0.85/25)	155	8.1	3415	13	75.9	184
			MINCAM1 (0.8/8)	1477	4.9	1084	17	81.5	459
		Ketzür/DE	REMO1 (0.8/8)	1467	6.5	5491	23	106.9	554
			REMO2 (0.8/8)	1478	6.4	4778	20	115.8	712
			REMO3 (0.8/8)	1420	5.6	1967	24	136.3	557
			REMO4 (0.8/8)	1478	6.5	5358	19	117.0	715
MORJO	Morvai	Fülöpszállás/HU	HUFUL (1.4/5)	2522	3.5	532	16	33.3	231
MOSFA	Moschini	Rovereto/IT	ROVER (1.4/4.5)	3896	4.2	1292	21	186.0	470
OCHPA	Ochner	Albiano/IT	ALBIANO (1.2/4.5)	2944	3.5	358	17	145.9	522
OTTMI	Otte	Pearl City/US	ORIE1 (1.4/5.7)	3837	3.8	460	23	168.8	324
PERZS	Perkó	Becsehely/HU	HUBEC (0.8/3.8)*	5498	2.9	460	21	121.3	632
ROTEC	Rothenberg	Berlin/DE	ARMEFA (0.8/6)	2366	4.5	911	14	75.8	129
SARAN	Saraiva	Carnaxide/PT	RO1 (0.75/6)	2362	3.7	381	28	243.6	590
			RO2 (0.75/6)	2381	3.8	459	27	238.3	869
			RO3 (0.8/12)	710	5.2	619	27	232.2	1036
			RO4 (1.0/8)	1582	4.2	549	26	179.9	366
			SOFIA (0.8/12)	738	5.3	907	26	248.5	664
SCALE	Scarpa	Alberoni/IT	LEO (1.2/4.5)*	4152	4.5	2052	16	108.0	230
SCHHA	Schremmer	Niederkrüchten/DE	DORAEMON (0.8/3.8)	4900	3.0	409	20	112.1	339
SLAST	Slavec	Ljubljana/SI	KAYAK1 (1.8/28)	563	6.2	1294	8	44.3	140
			KAYAK2 (0.8/12)	741	5.5	920	10	60.3	72
STOEN	Stomeo	Scorze/IT	MIN38 (0.8/3.8)	5566	4.8	3270	22	162.9	1249
			NOA38 (0.8/3.8)	5609	4.2	1911	21	166.4	1033
			SCO38 (0.8/3.8)	5598	4.8	3306	21	167.8	1148
STRJO	Strunk	Herford/DE	MINCAM2 (0.8/6)	2354	5.4	2751	22	114.4	557
			MINCAM3 (0.8/6)	2338	5.5	3590	20	101.8	332
			MINCAM4 (0.8/6)	2306	5.0	1412	22	87.7	139
			MINCAM5 (0.8/6)	2349	5.0	1896	19	98.4	311
			MINCAM6 (0.8/6)	2395	5.1	2178	21	109.9	278
TEPIS	Tepliczky	Agostyán/HU	HUAGO (0.75/4.5)	2427	4.4	1036	18	115.1	411
			HUMOB (0.8/6)	2388	4.8	1607	15	75.1	278
WEGWA	Wegrzyk	Nieznaszyn/PL	PAV78 (0.8/6)	2286	4.0	778	18	76.7	248
YRJIL	Yrjölä	Kuusankoski/FI	FINEXCAM (0.8/6)	2337	5.5	3574	11	51.0	181
ZAKJU	Zakrajšek	Petkovec/SI	TACKA (0.8/12)	714	5.3	783	13	94.0	183
* active field of view smaller than video frame						Overall	30	10 107.8	42 628

The International Meteor Organization

www.imo.net

Follow us on Facebook InternationalMeteorOrganization

Follow us on Twitter @IMOMeteors

Council

President: Cis Verbeeck,
Bogaertsheide 5, 2560 Kessel, Belgium.
e-mail: cis.verbeeck@scarlet.be

Vice-President: Juraj Tóth,
Fac. Math., Phys. & Inf., Comenius Univ.,
Mlynska dolina, 84248 Bratislava, Slovakia.
e-mail: toth@fmph.uniba.sk

Secretary-General: Robert Lunsford,
14884 Quail Valley Way, El Cajon,
CA 92021-2227, USA. tel. +1 619 755 7791
e-mail: lunro.imo.usa@cox.net

Treasurer: Marc Gyssens, Heerbaan 74,
B-2530 Boechout, Belgium.
e-mail: marc.gyssens@uhasselt.be
BIC: GEBABEBB
IBAN: BE30 0014 7327 5911
Bank transfer costs are always at your expense.

Other Council members:

Megan Argo, Jodrell Bank Centre for Astrophysics,
Alan Turing building, University of Manchester,
Oxford Road, Manchester, M13 9PL, UK.
e-mail: megan.argo@gmail.com

Javor Kac (see details under WGN)

Detlef Koschny, Zeestraat 46,
NL-2211 XH Noordwijkerhout, Netherlands.
e-mail: detlef.koschny@esa.int

Masahiro Koseki, 4-3-5 Annaka, Annaka-shi,
Gunma-ken 379-0116, Japan.
e-mail: geh04301@nifty.ne.jp

Sirko Molau, Abenstalstraße 13b, D-84072 Seysdorf,
Germany. e-mail: sirko@molau.de

Jean-Louis Rault, Société Astronomique de France,
16, rue de la Vallée, 91360 Epinay sur Orge,
France. e-mail: f6agr@orange.fr

Jürgen Rendtel, Eschenweg 16, D-14476 Marquardt,
Germany. e-mail: jrendtel@aip.de

Paul Roggemans, Pijnboomstraat 25, 2800 Mechelen,
Belgium, e-mail: paul.roggemans@gmail.com

Galina Ryabova, Res. Inst. of Appl. Math. & Mech.,
Tomsk State University, Lenin pr. 36, build. 27,
634050 Tomsk, Russian Federation.
e-mail: ryabova@niipmm.tsu.ru

Damir Šegon, J. Rakovca 3, 52100 Pula, Croatia.
e-mail: damir.segon@pu.t-com.hr

Commission Directors

Visual Commission: Rainer Arlt (rarlt@aip.de)
Generic e-mail address: visual@imo.net
Electronic visual report form:
http://www.imo.net/visual/report/electronic

Video Commission: Sirko Molau (video@imo.net)

Photographic Commission: Bill Ward
(William.Ward@glasgow.ac.uk)
Generic e-mail address: photo@imo.net

Radio Commission: Jean-Louis Rault (radio@imo.net)

Fireballs: Online fireball reports:
http://fireballs.imo.net

Outreach Officer

Jure Atanackov, e-mail: jureatanackov@gmail.com

Webmaster

Karl Antier, e-mail: webmaster@imo.net

WGN

Editor-in-chief: Javor Kac
Na Ajdov hrib 24, SI-2310 Slovenska Bistrica,
Slovenia. e-mail: wgn@imo.net;
include METEOR in the e-mail subject line

Editorial board: Ž. Andreić, M. Argo, D.J. Asher,
F. Bettonvil, J. Correira, M. Gyssens,
C. Hergenrother, T. Heywood, J.-L. Rault,
J. Rendtel, C. Verbeeck, S. de Vet, D. Vida.

IMO Sales

Available from the Treasurer or the Electronic Shop on the IMO Website	€	$
IMO membership, including subscription to WGN Vol. 46 (2018)		
Surface mail	26	35
Air Mail (outside Europe only)	49	65
Electronic subscription only	21	25
Proceedings of the International Meteor Conference on paper		
1990, 1991, 1993, 1995, 1996, 1999, 2000, 2002, 2003, per year	9	12
2007, 2010, 2011, per year	15	20
2012, 2013, 2014, 2015 per year	25	34
Proceedings of the Meteor Orbit Determination Workshop 2006	15	20
Radio Meteor School Proceedings 2005	15	20
Handbook for Meteor Observers	15	20
Meteor Shower Workbook	12	16
Electronic media		
Meteor Beliefs Project ZIP archive	6	8

2018 Perseids from Tepličné, Slovakia